Functional Roles of Two Chromatin Factors (USP22 and MENIN) in Reprogramming and Pluripotency

by

Mert GAYRETLİ

A Dissertation Submitted to the
Graduate School of Health Sciences

in Partial Fulfillment of the Requirements for

the Degree of

Master of Science

in

Cellular and Molecular Medicine

KOÇ
ÜNİVERSİTESİ

January 17, 2025

Functional Roles of Two Chromatin Factors (USP22 and MENIN) in Reprogramming and Pluripotency

Koç University

Graduate School of Health Sciences

This is to certify that I have examined this copy of a master's thesis by

Mert GAYRETLİ

and have found that it is complete and satisfactory in all respects,
and that any and all revisions required by the final
examining committee have been made.

Committee Members:

Prof. Tamer Önder

Prof. Tuğba Bağcı Önder

Assoc. Prof. Ali Cihan Taşkın

17.01.2025

ABSTRACT

Functional roles of two chromatin factors (USP22 and MENIN) in reprogramming and pluripotency
Mert GAYRETLİ
Master of Science in Cellular and Molecular Medicine
January 17, 2025

Overexpression of OCT4, SOX2, KLF4 and MYC (OSKM) factors can reprogram somatic cells to induced pluripotent cells (iPSC). Process of somatic cell reprogramming is inherently inefficient, pointing to the cell's intrinsic barriers that safeguards somatic cell identity. Previously conducted CRISPR-Cas9-based knockout screens during reprogramming revealed USP22 and MLL1 as barriers to reprogramming. In the first part of this thesis, overexpression of wild-type and catalytic mutant USP22 in USP22 KO cell lines were performed which showed that increased reprogramming efficiency is indeed related to USP22 loss, and this effect is not related to its deubiquitination activity. Reprogramming of USP22 knock-out primary fibroblasts under different primed pluripotency culture conditions proved that increased reprogramming efficiency is independent of cell line or culture condition of choice. Transcriptome analysis at specific time-points during reprogramming revealed that loss of USP22 represses fibroblast-specific genes such as COL1A2, POSTN, FOXC2 that occurs throughout reprogramming. In addition, USP22 loss results in upregulation of general pluripotency markers such as SOX2, LIN28A and naïve pluripotency markers such as DNMT3L, GDF3, ALPPL2, ARGFX as early as 3 days after OSKM expression. To investigate a potential role of USP22 in attaining naïve pluripotency, I reprogrammed somatic cells under naïve culture conditions which resulted in an increased number of naïve colonies as quantified by TRA 1-60/KLF17 double staining. In addition, USP22 loss enhanced conversion from primed to naive pluripotency indicated by higher expression levels of naive pluripotency markers DNMT3L and ALPPL2. In the second part of the thesis, I showed that MEN1 loss enhances reprogramming efficiency in primary fibroblasts. Rescue experiments utilizing overexpression of H433A mutant MENIN which cannot recognize H3K79me2, indicated that MENIN acts as a barrier partially through its ability to read this chromatin mark. To test whether knocking-out *MEN1* affects pluripotency, single clone iPSCs were generated from MEN1 KO fibroblasts. Characterization assays showed that these clones express endogenous OCT4, SOX2 and KLF4 while silencing C-MYC and other exogenous transgenes. Also, MEN1 iPSCs stably express pluripotency related proteins and contribute to all three germ layers when subjected to teratoma formation assay. Finally, MENIN-MLL1 Complex inhibition via VTP50469 enhanced reprogramming efficiency in primary fibroblast lines. In addition, VTP50469 supplementation increased reprogramming efficiency of 3-factor (OSK) reprogramming, and enabled iPSC generation with only 2 factos (OS). Taken together, this work demonstrates important roles for two distinct chromatin factors in reprogramming and pluripotency.

ÖZETÇE

İki kromatin faktörünün (USP22 ve MENIN) yeniden programlamada ve pluripotensideki fonksiyonel rolleri
Mert GAYRETLİ
Hücresel ve Moleküler Tıp, Yüksek Lisans
Ocak 17, 2025

OCT4, SOX2, KLF4 ve C-MYC (OSKM) faktörlerinin anlatımı somatik hücreleri uyarılmış pluripotent kök hücrelere (uPKH) yeniden programlayabilir. Somatik hücre kimliğini koruyan hücre içi bariyerlerin olması sebebiyle somatik hücre yeniden programlanması düşük verimli bir süreçtir. Daha önce gerçekleştirilen CRISPR-Cas9 bazlı susturma taraması ile *USP22* ve *MLL1* genleri yeniden programlama bariyerleri olarak ortaya çıkarıldı. Bu tezin birinci bölümünde, USP22 geni susturulmuş hücre hatlarının üzerine yabanıl tip ve katalitik mutant USP22'nin tekrar anlatılmasıyla, yeniden programlamadaki değişimin USP22 kaybıyla ilgili olduğu ve bu etkinin USP22'un katalitik aktivitesinden bağımsız olduğu kanıtlandı. USP22'nin fibroblast hücre hatlarında susturulması ve bu hatların farklı 'primed' kültür koşullarında yeniden programlanması ile, artan yeniden programlama veriminin hücre hattı ve kültür koşullarından bağımsız olduğu kanıtlandı. Yeniden programlamanın belirli zamanlarında yapılan transkriptom analizi, USP22'nin susturulmasının *COL1A2, POSTN, FOXC2* gibi somatik hücreye özgü genlerin yeniden programlama boyunca baskılanmasına yol açtığını ortaya çıkardı. Ek olarak, 3. gün gibi çok erken bir zamanda bile, USP22 kaybının *SOX2, LIN28A* gibi genel pluripotent genlerinin ve *DNMT3L, GDF3, ALPPL2, ARGFX* gibi 'naive' pluripotent genlerinin ifadesinin artmasına sebep olduğunu ortaya çıkarıldı. USP22'nin rolünün naive pluripotensiye ulaşmadaki rolünü araştırmak üzere somatik hücrelerden naive yeniden programlama deneyi yapıldı ve sonuç olarak TRA-1-60/KLF17 çift boyama ile belirlenen naive kolonilerin nicelik olarak arttığı gözlemlendi. Ek olarak, geçiş sırasındaki *DNMT3L* ve *ALLPL2* gibi naive pluripotensi genlerinin anlatımındaki artıştan yola çıkarak USP22 kaybının primed pluripotensiden naive pluripotensisine geçişin verimliliğini arttırdığı ortaya kondu. İkinci bölümde, *MEN1* geninin susturulmasının farklı fibroblast hücre hatlarında yeniden programlama verimini artırdığı gösterildi. H3K79me2 kromatin işaretini okuyamayan H433A nokta mutantı MENIN'in yeniden kurtarma deneylerinde kullanılmasıyla, MENIN'in yeniden programlamadaki bariyer fonksiyonunun kısmi olarak bu aktivitesiyle ilgili olduğu belirlendi. *MEN1*'in susturulmasının pluripotensiye etkisini kontrol etmek için, *MEN1* geni susturulmuş fibroblastlardan tek klondan büyüyen uPKH hatları üretildi. Karakterizasyon deneyleri bu klonların endojen *OCT4, SOX2* ve *KLF4* genlerini ifade ettiklerini, aynı zamanda transgenik *C-MYC* genini susturulduğunu gösterdi. Ayrıca, bu klonların stabil olarak pluripotensi ile ilgili proteinleri ifade ettiği ve teratom oluşumu deneyine tabii tutulduğunda, üç embriyonik tabakadan dokulara farklılaşabildiği gösterildi. Son olarak, VTP50469 kimyasalı kullanarak MENIN-MLL1 Kompleksi inhibisyonunun fibroblast hücre hatlarında yeniden programlama verimini artırdığı gözlemlendi. Ek olarak, VTP50469 3-faktörlü (OSK) yeniden programlamanın verimini artırdı ve yalnızca 2-faktör (OS) kullanarak uPKH üretimine olanak sağladı. Sonuç olarak, bu çalışma 2 farklı kromatin faktörünün yeniden programlama ve pluripotensideki önemli rollerini göstermektedir.

ACKNOWLEDGEMENTS

First, I would like to thank my advisor Prof. Dr. Tamer Önder, for giving me this opportunity to study in his lab. Trust and the independence he gave me while still providing scientific guidance when I need has been a great value for me to grow progress forward. As you are my first-ever PI, I will always be grateful for the chance you have given me.

Next, I would like to thank Alperen Yılmaz and Gülben Gürhan. We have worked on two projects together and potentially dozens more to come. I have learned a lot from both of you not only scientifically but also personally. Remembering the memories of memes we created and joyful laughs of Gülben during late-night experiments always brings a smile to my face. We shared countless fun moments together while keeping up with the pushy needs of Alperen. I look forward to work together with you in days to come.

I would like to thank Sıla Ünlü for being a super academic enthusiast. The positive mood you spread across the lab was the motivation I was looking for during my last semester. You will always be remembered as our fastest and loudest speaking friend, and we will always love it.

I would like to thank Elif Naz Ervatan for hard work and consistency. It will be enjoyable to watch you achieving great success during your career.

I would like to thank Deniz Örnek, Çağla Alagöz and Enes Sefa Ayar. Even though we are all in different continents now, I still feel your support.

I would like to thank friends from KUTTAM, Aksel, Beyza, Altar, Erdem, Gamze and Ezgi for coffee breaks and enjoying conversations.

I would like to thank my family Su Karakol, Cem Gayretli, İpek Poyraz and Volkan Poyraz for being constant pillars in my life even in the most stressful situations. You make my life infinitely better and easier; I feel blessed to have you as my core family.

Lastly, I would like to thank to my spouse Zülal Poyraz Gayretli, the amount of support you have given me during my grad years is beyond words. None of the good in my life would have been possible without your patience and guidance. You have been my strength and joy during the toughest moments. Thank you for being my love and my best friend.

I thank Associate Prof. İbrahim Kulaç from the Department of Pathology for his support in H&E staining and structural identification of teratomas.

This project has been supported, in part, by TUBITAK project no: 321S059.

TABLE OF CONTENTS

LIST OF TABLES

LIST OF FIGURES

ABBREVIATIONS

ICM	Inner cell mass
TSC	Trophoblast stem cell
ESC	Embryonic stem cell
PGC	Primordial germ cell
TF	Transcription factor
OSKM	Oct4, Sox2, Klf4 and c-Myc
iPSC	Induced pluripotent stem cells
MEF	Mouse embryonic fibroblast
MET	Mesenchymal-to-epithelial transition
SAGA	SPT-ADA-GCN5 acetylase
USP22	Ubiquitin specific peptidase 22
DMSO	Dimethyl sulfoxide protein
HENSM	Human Enhanced Naive Stem Cell Medium
Oct.04	Octamer-binding Transcription Factor 4
SOX2	SRY-box Transcription Factor 2
KLF4	Krüppel-like Factor 4
MEN1	Multiple Endocrine Neoplasia 1
MLL1	Mixed Lineage Leukemia 1
CRISPR	Clustered Regularly Interspaced Short Palindromic Repeats
HAT	Histone acetyltransferase
DMEM	Dulbecco's Modified Eagle Medium
PBS	Phosphate-buffered saline
KO	Knock-out
RT qPCR	Real time quantitative polymerase chain reaction
cDNA	Complementary DNA
Ct	Threshold cycle
TE	Trophectoderm
PSC	Pluripotent stem cell
HDAC	Histone deacetylase

VPA	Valproic acid
DUB	Deubiquitination
TGFB	Transforming Growth Factor Beta
ROCK	Rho-associated Kinase
LIF	Leukemia Inhibitory Factor
VPA	Valproic Acid
NaBut	Sodium Butyrate

CHAPTER 1:
INTRODUCTION

1.1 Stages of early embryonic development and embryonic stem cells

Embryonic development begins with fertilization which results in a first totipotent cell called zygote. The zygote undergoes a series of rapid mitotic divisions called cleavage, in which the number of cells increases while overall size and mass remains unchanged. When the resulting cell, known as blastomeres, reach 16 to 32 cells, they undergo compaction to generate the morula. As development progresses, around day 5 post-fertilization (dpf), morula undergoes a process called blastulation where cells contract and form a fluid-filled cavity called blastocoel. Contracted morula cells migrate to edges of the structure and form a ring of cells called trophoblasts (TB) and cells located inside at one pole of blastocyst called inner cell mass (ICM). This transition marks the first lineage segregation in early embryonic development (Rossant & Tam, 2022). Trophoblast cells are precursor cells of the placenta while ICM cells are precursors of the embryo proper. Blastocysts continue to expand until day 6 dpf when blastocyst reaches the uterus and initiates implantation process into endometrium. Implantation is a critical checkpoint in pregnancy, complications during implantation results in discontinued embryonic development (Shahbazi & Pasque, 2024).

Pre-embryonic development encompasses the period between fertilization and implantation. Embryonic development, on the other hand, begins with implantation, and continues until the 8th week of development. First critical event of the embryonic development occurs immediately after implantation that marks the second lineage segregation, where ICM cells positioned closer to trophoblast cells generate pluripotent epiblast cells and cells that position themselves closer to the blastocoel give rise to hypoblast cells. Following the ICM, trophoblast cells also differentiate into two layers called cytotrophoblast and syncytiotrophoblast. Once properly differentiated, syncytiotrophoblast begins secreting human chorionic gonadotropin hormone that maintains the pregnancy. As these cells grow and develop, specific signaling pathways are activated to prepare the embryo for gastrulation (Niakan et al., 2012). Around the third week of embryonic development, the pivotal process called gastrulation is initiated, during which, a bilaminar disk composed of epiblast and hypoblast develops into a trilaminar consisting of ectoderm, mesoderm and endoderm cells. While ectoderm and

mesoderm cells formed by epiblast precursors, endoderm lineage derived from hypoblast cells. Gastrulation is a critical stage that sets the foundation for neurulation and organogenesis (Zhai et al., 2021).

Studying human embryonic development presents several challenges including limited availability of embryos, the complexity of the experimental IVF procedures and ethical considerations. Consequently, the need for an in vitro model that is able to recapitulate events in embryonic development has resulted in the derivation of embryonic stem cells first from mice and then from early human embryos (Pera et al., 2000).

In 1981, two research groups led by Martin Evans and Gail Martin successfully derived first mouse embryonic stem cells (mESC) from 3.5 dpf stage blastocysts (Evans & Kaufman, 1981). Procedure involved natural mating or in vitro fertilization of specific mouse strains followed by sacrificing mated female at 3.5 dpf to collect blastocyst from uterus. Then, the collected blastocyst cultured in drops of medium under paraffin oil. Trophoblast cells show more adherence to culture dishes compared to ICM cells which form egg-cylinder-like cells at this time point. These structures are enzymatically dissociated with trypsin and then plated on mitomycin C treated mouse embryonic fibroblast (MEFs) feeder layer under specific culture conditions that includes serum and leukemia inhibitory factor (LIF). Characterization of mESCs was conducted regularly including having small round compact colonies as morphology, activated pluripotency markers like Oct4, Sox2, Nanog in the context of both proteome and transcriptome. In addition, cells are functionally characterized by their ability to form teratoma upon injection to mice and develop embryoid bodies in vitro while maintaining normal karyotype.

Seventeen years after first mESC derivation, in 1998, first human embryonic stem cells were derived by a group led by James Thomson. Group is successfully derived 5 cell lines; H1, H7, H9, H13, H14 from 36 embryos derived from in vitro fertilization clinics. Procedure involved, immunosurgery-based extraction of cells from ICM compartment which were then plated onto a MEF feeder layer in serum-containing media (Thomson et al., 1998).

1.2 Somatic cell reprogramming

In 1940, Conrad Waddington proposed the metaphorical diagram called epigenetic landscape. In his diagram, Waddington described how cells differentiate in the progress

of development, as balls rolling down the hills while reaching different valleys according to their different cell fates. As cells go down, they lose their plasticity and hills between valleys become higher and more visible meaning that cells become restricted to a certain somatic identity (Waddington, 1957). It is one of the foundational concepts in developmental biology and most of the arguments regarding this metaphor are still relevant today, however, Waddington depicted cell differentiation as rigid irreversible phenomena which is challenged by the finding of somatic cell reprogramming. First, in 1962, John B. Gurdon showed that transplanting the nucleus of an intestinal epithelial frog cell into an enucleated frog egg can properly undergo development resulting in a fully capable tadpole (Gurdon, 1962). With this work called Nuclear Transfer, Gurdon proved that differentiated somatic cell identity is not an irreversible state and can be reversed back to high potency state under certain conditions. Process is called nuclear transfer and becomes the groundwork for cell plasticity and reprogramming. Following Gurdon, in 2006, Yamanaka and colleagues hypothesized that factors that play a critical role in pluripotency networks in embryonic stem cells (ESCs) might ignite this network de novo and reverse their somatic cell identity into pluripotent state. They selected 24 candidates from this network and used a reporter-based screen approach to narrow down the pool of candidates. They identified 4 transcription factors (after called Yamanaka factors) that upon overexpression can reprogram the mouse fibroblast cells into pluripotent cells. After successfully generating mouse iPSC, the same group also reported iPSCs, generated from human fibroblast cells (Takahashi & Yamanaka, 2006). With these two seminal works that were awarded Nobel Prize in 2012, the field of developmental biology came to consensus that lineage specific cell fates are not permanent and indeed can be reversed back to pluripotency.

Somatic cell reprogramming is a multi-step transition process where somatic cells undergo major molecular and epigenetic changes. Somatic cells engage the process with an initiation phase, characterized by features like rapid proliferation and mesenchymal-to-epithelial transition (MET). MET is considered as a milestone for a somatic cell to break from somatic identity and enter the transient state for reaching pluripotency afterwards (Lai et al., 2020). The next phase (maturation) is characterized by activation of early pluripotency genes that results in changes in regulating key developmental genes. In this phase, as early pluripotency genes become activated, developmental genes that are hard to access in somatic cells become available epigenetically and genes relating to somatic cell identity becomes more inaccessible. Stabilization is the final phase of

reprogramming characterized by complete activation of the pluripotency core network and full resetting epigenetic memory of somatic cell identity. Additionally, transgenes that initiate the reprogramming are silenced in this phase meaning that stabilization is the phase when cells transition from exogenous transgene induction dependent state to more endogenous dependent (autonomous) state (Buganim et al., 2013).

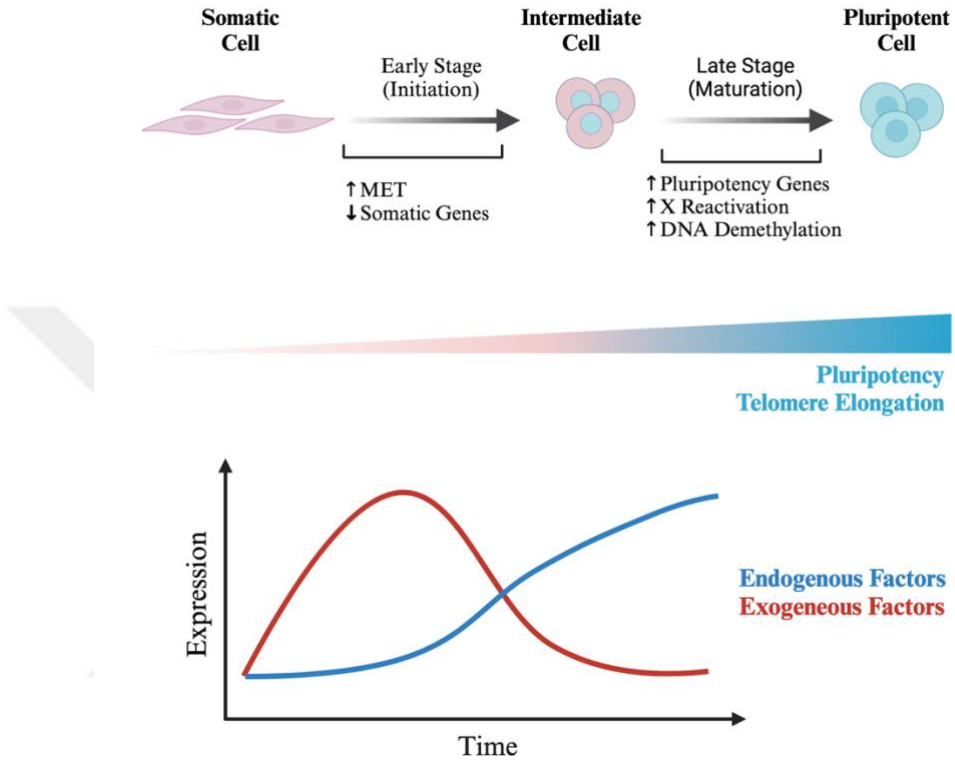

Figure 1.1. Stages of Somatic Cell Reprogramming (Figure adapted from Takahashi & Yamanaka, 2015)

Modification in epigenetic landscape during reprogramming plays a crucial role in cells losing their somatic cell identity and acquiring pluripotent state. Epigenetic remodeling is initiated by OSKM transcription factors, where they bind to specific pluripotency related loci and recruit epigenetic modifiers. Enhancers and promoters of pluripotency related genes are deposited with Histone marks that decondense the chromatin such as H3K4me3 and H3K27ac while histone marks condensing the chromatin including H3K27me3 and H3K9me3 are erased. Epigenetic remodeling occurs conversely for the genes associated with somatic cell identity. More specifically, in the maturation phase of reprogramming, demethylation of promoters of pluripotency related genes and hypermethylation of somatic gene promoters is established to achieve self-sustaining pluripotent state.

Induced pluripotent stem cell (iPSC) technology offers a variety of opportunities in biotechnology and regenerative medicine. Since reprogrammed cells can differentiate any type of cells within any tissue, they enabled damaged cell or tissue replacement, personalized cell therapies that minimize the risk of immune rejection (Cerneckis et al., 2024). Disease modelling is another application of iPSC technology, since the reprogrammed cells retain the genetic background of an individual completely, it allows researchers to study complex disorders. Beyond applied sciences, iPSC technology also contributes to basic research by generation of organoid structures that aim to recapitulate different tissue organizations (Lehmann et al., 2019).

1.3 Dynamic states of pluripotency

Early embryonic development is highly dynamic, occurring in a fast-paced environment that results in a diverse array of cells with distinct transcriptomes and metabolic signatures. These dynamic pluripotency states coincide with cellular characteristics of unique stages of early embryonic development. Although there are several states in the pluripotency spectrum, mainly two primary pluripotent states are characterized as naive and primed pluripotent states exhibiting distinct cellular and functional features (S. Takahashi et al., 2017). In terms of their developmental origin, naive pluripotency reflects the characteristics of inner cellular mass (ICM) of pre-implantation blastocyst, whereas primed cells correspond to post-implantation epiblast cells (Weinberger et al., 2016). In terms of developmental potential, functional studies that include implanting pluripotent cells into the ICM of developing blastocyst show that naive pluripotent cells (nPSC) are able to contribute to chimera formation with high efficiency whereas primed pluripotent cells (pPSC) fail to do so. The epigenetic landscape also differs between two states, nPSC exhibits a global hypomethylated genome that results in overall more accessible epigenetic configuration where both X chromosomes remain active. In pPSC however, epigenetic configuration is more restricted, characterized by higher levels of methylated regions across the genome. nPSCs are also different from pPSCs in terms of metabolic profiles; pPSC can only utilize glycolytic metabolism for energy production whereas nPSC utilizes both glycolysis and oxidative phosphorylation. Different in vitro characteristics are also observed between two states. nPSC shows dome-shaped colony morphology and are resilient when dissociated into

single cells, whereas pPSC exhibit flattened, monolayer-like morphology and are prone to apoptosis or differentiation when dissociated into single cells (Du & Wu, 2024).

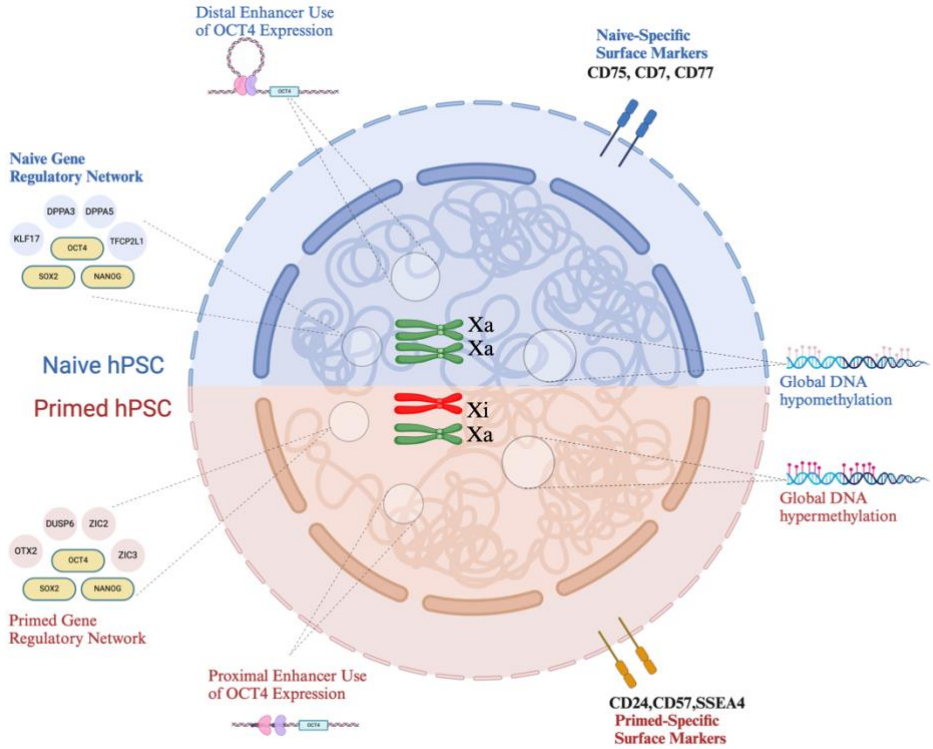

Figure 1.2. Distinct features of primed and naïve pluripotency (Figure adapted by Collier and Rugg-Gunn (2018))

To sustain their potency and self-renewal, human pPSC relies on two critical signalling pathways: FGF/ERK and TGFβ/Activin/Nodal pathways. FGF2 (Basic fibroblast factor 2) serves as a ligand for FGFR (Fibroblast Growth Factor Receptor), that upon activation, results in induction of PI3K/AKT, PLCγ and MEK/ERK downstream signaling pathways. Activating PI3K/AKT pathway suppresses differentiation and maintains self-renewal through regulating pluripotency genes like SOX2. Furthermore, studies show that inhibiting the PI3K/AKT pathway causes rapid apoptosis of pPSC, which highlights the pivotal role for cell survival. In addition, through regulating intracellular calcium transfer, PLCγ pathway is required for maintaining primed pluripotency. Through interacting with TGFβ/Activin/Nodal pathways and through regulating transcription factor NANOG, high basal MEK/ERK signaling pathway activity is required for sustaining primed pluripotency. Upon activation of the TGFβ/Activin/Nodal signaling, SMAD2 and SMAD3 proteins are phosphorylated and

make a complex with SMAD4 protein that translocates to the nucleus. This complex interacts with the regulatory sequences of pluripotency genes, primarily NANOG and forms a positive feedback loop that is essential for maintenance of primed pluripotency. In addition, studies show that inhibition of TGFβ/Activin/Nodal signaling results in low basal NANOG expression causing differentiation primarily through neuroectoderm lineage fate (Dalton, 2012).

Naïve pluripotency in mouse embryonic stem cells (mESC) is regulated through complex interactions between signaling pathways. These cells rely mainly on LIF/STAT3, BMP4 signaling, Wnt/β-Catenin and MAPK/ERK Pathways. Leukemia Inhibitory Factor (LIF) is a cytokine that triggers the activation of JAK Kinases, which in turn results in phosphorylation of STAT3. Activated STAT3 relocates to the nucleus and cooperating with NANOG, it directly regulates key naive pluripotency genes like Klf4 and indirectly upregulates the other transcription factors essential for naive pluripotency network like Tfcp2L1, Gbx2 and Sall4 (Yamane et al. 2018). Wnt/β-Catenin also plays a crucial role in maintaining naive pluripotency through transcriptional control. Upon binding of Wnt proteins to their corresponding receptors, GSK3 inhibition takes place that leads to stabilization of β-Catenin. Stabilization leads to accumulation in the cytoplasm that causes β-Catenin to relocate to the nucleus and interact with LEF/Tcf transcription factors that eventually activate target pluripotency genes. In addition, β-Catenin forms complexes with CREB-binding proteins (CBP) in the nucleus that cause upregulation of OCT4 and NANOG expression (Miyabayashi et al., 2007). Wnt activation through GSK3 inhibition is required for prevention of primed transition and maintain naive state (Dong et al., 2019). Although high basal activation of ERK is required for primed pluripotency, it is shown that phosphorylated ERK is detrimental for naive states suggesting its dual role between pluripotent states. High ERK signaling directly downregulates NANOG expression that results in breakdown of naive state pluripotency network (Stuart et al., 2014). Overall, combining GSK3 inhibitor, MEK/ERK inhibition is required to achieve the ground state.

Although signaling regulation of naive pluripotency and in vitro culture conditions to maintain this state is well established, human naive pluripotency is still an active research area. First human naive acquisition was reported in 2010 by Jacob Hanna from Rudolf Jaenisch's Lab. Their study suggests that naive characteristics observed in mESC can be achieved through transient activation of Oct4, Klf4 and Klf2 followed by a culture with ERK inhibition (PD0325901), GSK3 inhibition (CHIR99021), LIF and Forskolin

introduction. With this finding, they suggest that human pluripotent cells can achieve a naive state *in vitro* but the process requires more detailed chemical manipulation (Hanna et al., 2010).

In 2014, Austin Smith's group reported a naive conversion approach including overexpressing KLF2 and NANOG (Takashima et al., 2014). They first utilize the dox-inducible system to activate the naive pluripotency network, followed by culturing them in mouse naive conditions which includes MEK/ERK inhibitor (PD0325901), GSK3 inhibitor (CHIR99021) and JAK-STAT activator (LIF) with the addition of PKC inhibitor (Gö6983). In 2017, a report from the same group showed that naive pluripotency can be achieved without any genetic manipulation (Guo et al., 2017). They reported a protocol which initially exposed the primed human pluripotent cells with histone deacetylase inhibitors (VPA or NaBut) for 3 days and then introduce a mixture of inhibitors and cytokines called PXGL which includes MEK/ERK inhibitor (PD0325901), XAV939(WNT inhibitor), PKC inhibitor (Gö6983), JAK-STAT activator (LIF). All stages of this protocol require MEFs as a feeder layer. They also reported that stabilization of naive pluripotency state is achieved by cells with PXGL media for 5-15 passages.

More recently, Hanna lab reported a media with inhibitors and cytokines that enables both transgene free and feeder free conditions. The media called Human Enhanced Naive Stem Cell Medium (HENSM) includes MEK/ERK inhibitor (PD0325901), XAV939 (WNT inhibitor), PKC inhibitor (Gö6983), JAK-STAT activator (LIF), CGP77675 (SFK inhibitor), Y27632 (Rho-associated Kinase inhibitor), BIRB796 (p38-MAPK inhibitor), Activin A and Geltrex. Since hypomethylation is another issue reported for naive cultures, replacing HDACi with other chemicals also improves chromosomal stability (Bayerl et al., 2021).

1.4 Chromatin-based barriers to reprogramming

The efficiency of transcription factor-based reprogramming is remarkably low, with only 0.01 to 0.1 % of cells reaching pluripotency, pointing to the presence of the cell's intrinsic barriers to reprogramming (Arabacı et al., 2020). These barriers are primarily chromatin-based and can be categorized into two types: repressive chromatin marks and chromatin modifications associated with active transcription. Repressive histone modifications such as DNA Methylation, H3K9 methylation, histone deacetylation and variant histone deposition act as a barrier by preventing the activation of pluripotency

related genes (Apostolou & Hochedlinger, 2013). DNA Methylation acts as a barrier through multiple mechanisms: Methylation at CpG islands blocks transcription factor binding to regulatory elements such as enhancers and promoters. Additionally, through methylation, methyl-CpG binding (MBD) proteins are recruited to genomic regions which further repress the transcription. Various approaches have been developed to overcome DNA Methylation-based barriers to reprogramming including introduction of DNA Methylation inhibitors such as 5-azacytidine or forced overexpression of DNA demethylases like TET enzymes (De Carvalho et al., 2010). H3K9 modification accumulates around pluripotency-related genomic regions and forms an obstacle-like structure called refractory domain that blocks the OSKM factors from binding and activating genes located around these regions. Maintenance of the H3K9 repressive mark is facilitated by a complex that includes two main methyltransferases: SUV39H1 and G9a (Popowski, 2015). Conversely, chromatin marks associated with active transcription are also barriers to somatic cell reprogramming by maintaining the high expression of somatic identity-related genes (Ehrensberger & Svejstrup, 2012). One such modification is the H3K79 methylation, an active histone mark catalyzed by DOT1L, which serves as a barrier through maintaining somatic identity gene expression programs. Chemically inhibiting catalytic activity of DOT1L that enables silencing of somatic gene expression programs, thereby enhancing reprogramming efficiency (Onder et al., 2012). H3K27ac is another active histone mark that plays a role in maintaining proper expression levels of somatic cell identity genes in mammalian cells. Acetylation of histones are regulated through an interplay between histone acetyltransferases such as p300/CBP and histone deacetylases. The barrier function of this acetylation mark can be overcome through inhibiting such acetyltransferases (Ebrahimi et al., 2019).

Overall, strategies that involve reducing the chromatin marks that are associated with active transcription of somatic cell identity genes and diminishing the chromatin modifications that repress transcription of pluripotency-related genes results in a higher efficiency somatic cell reprogramming.

1.5 Screen approaches for identifying barriers to somatic cell reprogramming

A variety of screening approaches have been conducted to study the barriers to somatic cell reprogramming in mammalian cells. Among these, genome-wide screens that utilize RNA interference for perturbation have proven particularly impactful. In a mouse study, a genome-wide shRNA screen identified several novel barriers, including Arx, Ankrd22, Cdkn2aip, Erf, Foxn3, Hoxd4, Hoxd12, Tfdp1, Gtf2e1, Nfe2 (Qin et al., 2014). In the same year, a human genome-wide shRNA study identified barriers to human somatic cell reprogramming, including a family of transmembrane and their secreted proteins known as disintegrin metalloendopeptidases (ADAM family proteins) such as ADAM7, and ADAM21. Other notable findings included transcription factors such as TTF2, TMF1, as well as chromatin regulators such as ATF7IP and MED19 (Yang et al., 2014).

Genome-wide perturbation screens have revealed that epigenetic modifiers play a significant role in determining reprogramming efficiency. Consequently, several other screens have specifically targeted epigenetic modifiers rather than entire genomes. In 2012, Onder et al. conducted an shRNA screen specifically targeting chromatin modifiers and identified DOT1L, a H3K79 methyltransferase as a barrier to reprogramming (Onder et al., 2012). Using similar shRNA screening approaches other research groups identified additional epigenetic modifiers as barriers to reprogramming, including SETDB1, which deposits H3K9me3 marks on somatic cell related genomic regions (Miles et al., 2016). Collectively, these findings underscore the indispensable role of chromatin modifiers in the process of somatic cell reprogramming.

CRISPR-Cas9 system is also utilized to identify barriers to reprogramming. In 2017, a group developed a unique approach called CRISPR-UMI screen (Michlits et al., 2017). To overcome the limitations of traditional CRISPR-Cas9 screening, they tagged each cell with unique molecular identifiers (UMIs) that enabled them to track the cells at clonal level, decreasing the risk of false positives. In this mouse study, novel barriers to reprogramming such as Pias1, Men1, Senp1, Uba2 and Sae1 are identified alongside known barriers like Trp53, Pten, Dot1l, Socs3 and Chaf1a.

More recently, our group had conducted a perturbation-based CRISPR-Cas9 screening approach designed specifically for human somatic cell reprogramming. Using a focused gRNA pool, they had targeted the coding regions of 247 histone modifier genes. For each gene, 5 to 10 gRNAs were utilized with the addition of 80 non-targeting gRNAs

as a control. Each gRNAs were cloned into a Cas9-expressing plasmid, followed by lentiviral packaging and transduction into human fibroblasts. The transduced cell lines were reprogrammed using OSKM factors supplemented with a DOT1L inhibitor, a known enhancer of reprogramming efficiency. On Day 14 of reprogramming, TRA-1-60 (a surface marker for pluripotency) positive cells were sorted, and their genomic DNA was extracted. Sequencing adapters were added to the gRNAs through PCR amplification. Then, each fragment was sequenced, and gRNA sequences were aligned to the whole genome. The MaGECK algorithm was utilized to identify enriched gRNAs by comparing their representations between Day 0 and Day 14 TRA 1-60 positive sorted cells. Along with previously known chromatin modifiers, new barriers such as USP22 and MLL1 had been identified (Aztekin, 2016).

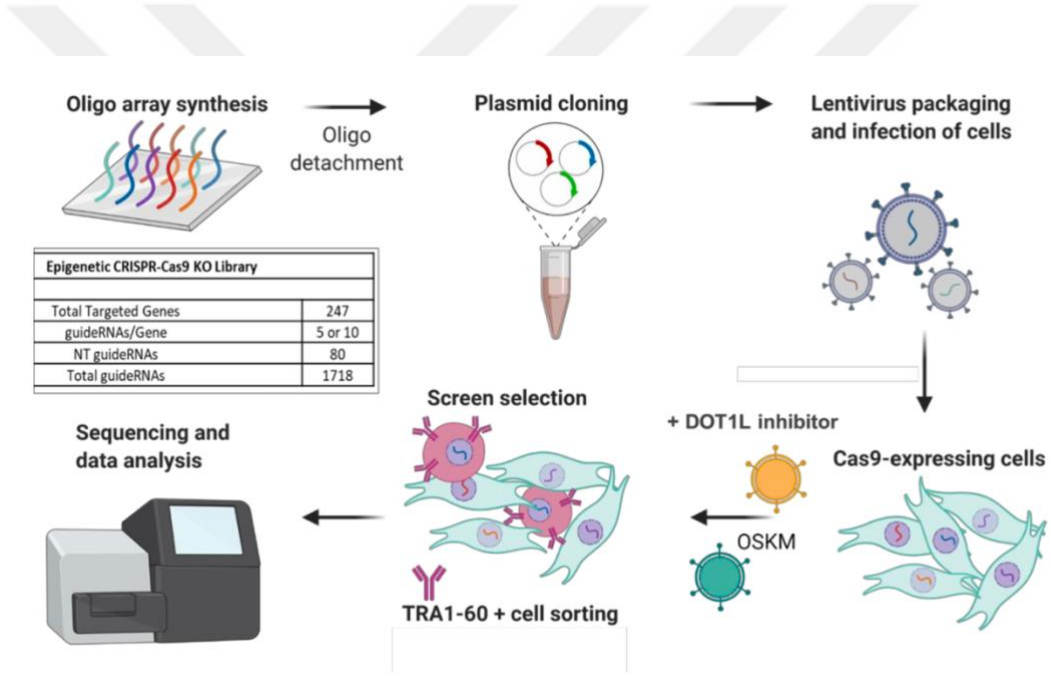

Figure 1.3. Schematics of CRISPR-Cas9-based Screening Approach.

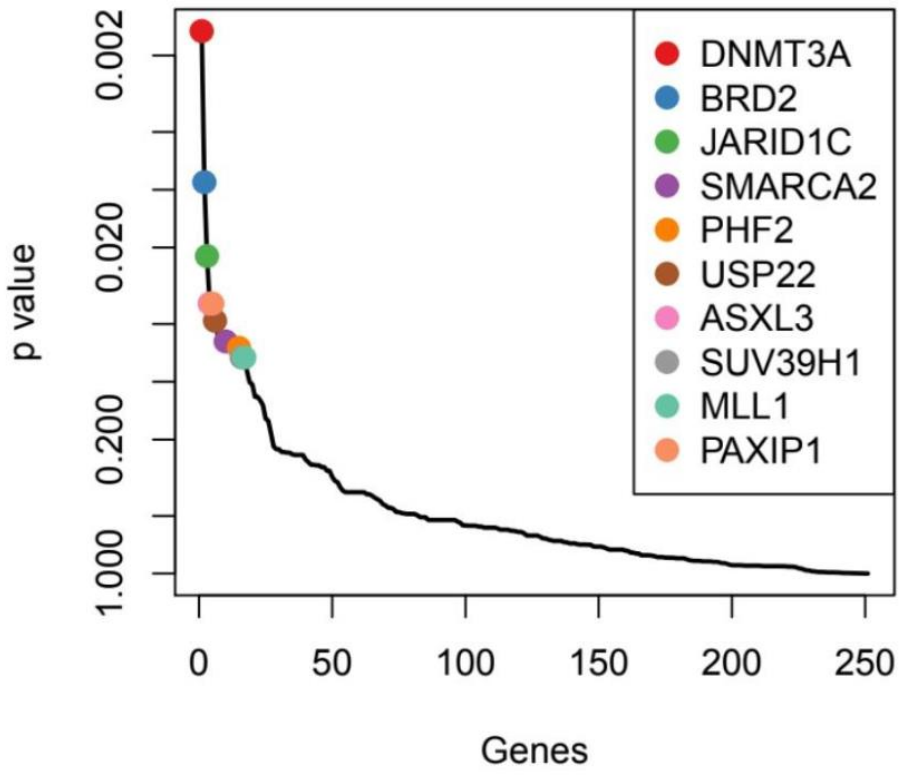

Figure 1.4. Positively enriched sgRNAs from Day 14 of Reprogramming

1.6 USP22, MENIN and MLL proteins

Post-translational modifications are the mechanisms for the cells to regulate protein's activity, localization and stabilization. One of these modifications is ubiquitylation, which involves adding a small protein of ubiquitin to specific lysine (K) residues of targeted protein. The addition of ubiquitin causes diverse responses from cell machinery depending on the specific site of this modification and number of ubiquitin proteins to attach (Melo-Cardenas et al., 2016). For instance, ubiquitination at lysine (K48), marks the protein for proteasome-mediated degradation, wherein proteasome recognizes and breaks down ubiquitin-tagged protein into smaller peptides that are reusable for cellular machinery. This modification is carried out by three distinct enzyme groups: E1s (ubiquitin activating enzymes), E2s (ubiquitin conjugating enzymes), E3s (ubiquitin ligases), each having unique roles in ubiquitination process (Glickman & Ciechanover, 2002). The enzyme group that counters the activity of these ubiquitous enzymes are known as deubiquitylates (DUBs). DUBs cleave the amide bond between ubiquitin and the protein, resulting in detaching the ubiquitin tag from protein. DUBs are

sub-grouped into 6 families. Among these families, the largest one is called ubiquitin-specific proteases (USPs) (Reyes-Turcu et al., 2009). USP22, yeast ortholog is called Ubp8, is one of the members of USPs family and it is highly conserved from yeast to vertebrates. Crystal structure of USP22 revealed that it contains two distinct domains, a zinc finger domain at the N-terminus, which is required for DNA binding and a catalytic domain at C-terminus (Daniel & Grant, 2007). Catalytic domain is composed of three subdomains-fingers, palm and thumb. Protease active domain of USP22 is located between Palm and the Thumb (Bonnet et al., 2008).

SAGA is a transcriptional coactivator complex consisting of multiple modules each having distinct functions. It has been shown that SAGA Complex regulates gene expression through its catalytic modulus: the HAT (histone acetyltransferase module) and the DUB (Deubiquitinase Module). In addition, two other domains which have no catalytic activity: the TF binding module and the core structural module. SAGA is an evolutionary conserved complex that is considered irreplaceable for differentiation, growth, immune response and other fundamental aspects of eukaryotic life (Lang et al., 2011). Co-immunoprecipitation studies showed that USP22 is the component of SAGA's DUB module. Studies on catalytic mutant USP22 reveals that H2BK120 ubiquitination is absent in these mutants and research on mechanism of DUBs suggests that they can regulate activities of important signaling pathways such as p53, Wnt, EGFR and NF kB (Sowa et al., 2009).

MENIN is a protein encoded by the *MEN1* (Multiple Endocrine Neoplasia Type 1) gene. Patients with Multiple Endocrine Neoplasia Type 1 disease which is characterized by tumor occurrence in multiple endocrine tissues (predominantly parathyroid), are found to harbor mutations in the *MEN1* gene. Patients with MEN1 syndrome usually carry heterozygous germ-line mutation, followed by loss of other somatic copy resulting in the production of completely functionless MENIN protein (Matkar et al., 2013). Features of *MEN1* syndrome suggest that MENIN acts as a tumor suppressor in endocrine tissues. Mouse models provide a platform for studying the characteristics and mechanisms of tumor formation. In one study, researchers generated mice with heterozygous loss and homozygous loss of Men1 gene. They observed that homozygous loss was embryonic lethal resulting death between embryonic day 11 to 14.5 whereas heterozygous loss model survives the gestation but around 10 months after birth, tumor occurrence is observed in endocrine tissues, which is a pattern also observed in humans (Piret & Thakker, 2011b). Additionally, liver-specific mutations in the Men1 gene did not cause any tumor

formation, suggesting tissue specific tolerance to Men1 loss. These studies show us the importance of Menin in embryonic development and its function as a tumor suppressor (Piret & Thakker, 2011).

Crytsal structure of Menin revealed a “curved left hand” with interacting “palm” and “thumb”-like regions. Among the various domains of Menin, three tetratricopeptide (TRP) motifs are of particular interest. Proteins with scaffold features which provide a platform for protein-protein interactions are known to have TRP motifs (Murai et al., 2011). Evidence for enzymatic activity of Menin has not been demonstrated. Therefore, to uncover physiological roles Menin plays in organisms, studies have focused on its interaction partners and which signaling pathways are affected through these interactions. Menin interacts with a variety of partner proteins, including transcription factors, epigenetic regulators and proteins involved in responses to DNA damage (Huang et al., 2012). Menin’s interactions with transcription factors are particularly important since through these interactions, Menin can act both as activator and repressor depending on the interaction partner it binds. Multiple protein-protein interaction studies have shown JUND is one of the specific and direct interaction partners of MENIN. JUND interacts with MENIN through its N terminus region. Directed mutations to this binding region disrupts the interaction between JUND and MENIN. Additionally, through interacting with JUND, MENIN primarily functions as a transcriptional repressor. Together with JUND, Menin forms a complex with mSin3A and HDAC. They reduce the acetylation of JUND targets (e.g gene Gastrin) and therefore reduce their expression (Agarwal et al., 1999). Alternatively, Menin occupies the phosphorylatable N-terminal region of JUND, preventing c-Jun N-terminal Kinase (JNK) from phosphorylating the region, thus preventing the JUND from being activated. Together with Menin, JunD binds to the promoter region of the Gastrin gene to suppress its expression. Additionally, a mouse study conducted with JUND-G42E which is a mutant JUND deficient for Menin binding, eliminates the growth suppress effect of JUND and makes it a growth promoting protein (Gobl et al., 1999). Together, these studies highlight the importance of Menin-JUND interaction for the tumor suppressor function of Menin protein.

Menin regulates multiple signaling pathways through both direct and indirect interactions. For instance, NF-kB pathway is repressed by Menin through the recruitment of Sirt1 which deacetylate lysine 310 of p65 which is the one of the critical components of this pathway. The TGF-β pathway is another signaling cascade regulated by Menin which interacts with the SMAD3, component of TGF- β. Studies on mouse parathyroid

cells suggest bidirectional regulatory relationship between Menin and TGF- β signaling pathway (Rulifson et al., 2007).

In a recent study, Menin was characterized as a reader of H3K79me2 histone mark that involves gene expression regulation. Using a combined approach of proteomics and nucleosome-based probing, the authors showed that Menin is able to specifically bind H3K79me2 by utilizing its fingers and palm domains which together creates π-cation interaction with its H433 residue. In addition, using cryo-EM, they analyzed the structure of the Menin during H3K79me2 recognition and found that it simultaneously interacted with MLL1 meaning Menin has separate binding pockets for nucleosomes and other transcriptional regulators. Finally, they suggest that loss of H3K79me2 which is induced by introducing a DOT1L inhibitor results in disruption of Menin's interaction with chromatin thereby reducing gene expression of Menin targets (Lin et al., 2023).

Mll1 is another critical interaction partner of Menin. Mass Spectrophotometry-based studies on two MLL complexes (one consists of Mll1 and other Mll2) have revealed that Menin is a component of both complexes (Yokoyama et al., 2004). Both complexes are shown to exhibit histone methyltransferase activity responsible for specific covalent histone modification on trimethylated histone H3 on lysine 4. H3K4me3 is shown to have a positive effect on transcription of modified regions. Studies on Menin mutants that are identified from patients with MEN1 syndrome deficient in MLL interaction show lower HMTase activity that in turn cause loss of activating marker and repress transcription. MLL1 also regulates hematopoietic differentiation by modulating subsets of HOX genes. Translocation in the MLL gene causes upregulation of other members of HOX family proteins such as HOXA7 or HOXA9 which disrupts the physiological differentiation and drives leukemogenesis. Menin acts as an oncogenic cofactor for MLL fusion protein resulting from MLL gene translocation (Yokoyama & Cleary, 2008). These findings highlight the dual role of Menin as both tumor suppressor and an oncogene.

Knowing that the Menin-MLL interaction is crucial for leukemogenesis, researchers developed a way to inhibit this interaction. Using a structure-based drug design approach, chemical VTP50469, a highly potent, selective small molecule inhibitor for Menin-MLL interaction was developed. Inhibitor successfully displaced the Menin from MLL fusion complexes which results in MLL being unable to bind the chromatin related to its targeted genes (Krivtsov et al., 2019).

In the first part of this thesis, I showed USP22 is a barrier to reprogramming independent of its ubiqutinate activity. Using time-course transcriptome analysis I

showed that USP22 impedes reprogramming by safeguarding the somatic cell identity related genes and preventing expression of pluripotency related genes throughout the reprogramming process. In addition, USP22 loss also enhanced somatic cells to reach pluripotency with higher potency called the naive state. Finally, I also hypothesized that USP22 might have a repressive role within pluripotency. To test that, I performed naive conversion of USP22 knockout primed iPSCs and showed that a subset of naive pluripotency markers is upregulated during the first 6 days of conversion.

In the second part, I showed that MEN1 loss and MENIN-MLL1 Complex inhibition by VTP50469 independently enhances reprogramming efficiency in primary fibroblast cell lines. I also performed rescue experiments utilizing the MENIN point mutant which is deficient for recognizing H3K79me2(Lin et al., 2023). This mutant can only partially rescue the MEN1 KO phenotype suggesting that H3K79me2 reading activity is related to MENIN's barrier function to reprogramming. Finally, I showed that VTP50469 supplementation enables 2-factor (OS) reprogramming.

CHAPTER 2:
MATERIALS AND METHODS

2.1 Cloning and transformation

LentiCRISPR-v2 (Addgene plasmid, #52961) plasmid was enzymatically digested with BsmB1 (NEB). Then, digested plasmid was run on gel electrophoresis followed by purification using MN PCR Clean Up and Gel Extraction Kit (Macherey-Nagel™ cat. #740609.50). Purified linear vector was treated with Antarctic Phosphatase (NEB, cat. #M0289S). Top and bottom guide RNA sequences were taken from GeCKO Library. Using T4 Polynucleotide Kinase (3' phosphatase minus,NEB) and T4 DNA Ligase Buffer (NEB) mix, each top and bottom gRNA oligo was annealed. The reaction mixes up to 10 µl was incubated at 37°C for 30 minutes, followed by 95°C for 4 minutes, then temperature was ramped down from 95°C to 25°C with the rate of 5 °C/min in a thermal cycler. Annealed oligos were diluted with the ratio of 1:200, then used as an insert for the LentiCRISPR-v2 vector. 50 ng of LentiCRISPR-v2 plasmid was used for a ligation reaction which was incubated at RT for 2 hours. Then, competent bacteria were thawed in ice. From each ligation sample, 5 µl was transferred to 50 µl competent bacteria followed by 30 minutes incubation on ice. After incubation, heat shock protocol was performed by putting each mix into a 42°C water bath for 30 seconds followed by 5 minutes incubation on ice. 150 µl SOC medium was added to each mixture and cultured at 37°C in an orbital bacterial shaker at 225 rpm for 45 minutes. 100 µl from cultured mix was spread on Ampicillin resistant LB agar plate. Cloning was validated using Sanger sequencing with primers targeting the U6 promoter (Yilmaz,2023) (Gürhan, 2023).

Table 2.1: Table of guide RNAs used for cloning (Yilmaz,2023) (Gürhan, 2023)

USP22_1_Top	CACCGAGTCCCGCAGAAGTGGCGTG
USP22_1 _Bottom	AAACCACGCCACTTCTGCGGGACTC
MEN1_2_Top	AAACTGTCTGAGGATCATGCCTGGC
MEN1_2_Bottom	CACCGCCGGTAGCGTAGCAAATGGC

To generate USP22 g1 and MEN1 g2 resistant cDNAs, point silent mutation was performed to change the NGG site (PAM sequence) on Flag-HA-USP22(Addgene plasmid, #22575) (Gürhan, 2023) and pBABE Hygro WT MEN1 (Addgene plasmid, #11024) respectively (Yilmaz,2023). To do it, Q5 site directed mutagenesis kit (NEB, cat. # E0554S) was used with appropriate primers listed.

Table 2.2: Table of Primers used for Q5 based site directed mutagenesis

Q5-22575-USP22g1-F	GTGGCGTGTGTGTCAGGGCCT
Q5-22575-USP22g1-R	TTCTGCGGGACTTCTTCCTG
Q5-22575-C185A-F	GTTCATGAAGGCTGTGTTCCCAAGGTTG ATCAGCC
Q5-22575-C185A-R	TGCATCGTGCAGGCCCTG
MEN1_11024_PAM_Mutation_F	TGTCCACCTCGCACTGTCTGAGG
MEN1_11024_PAM_Mutation_R	TCCCGGAGACCCAGGGCC
MEN1-H433A-F	GCGGTGGGCTGGGCCACCTTTC
MEN1-H434A-R	CAGCACAGGCGTGGGAC

2.2 Plasmid DNA isolation

Single bacteria colonies grown in LB Agar Plates are picked and incubated as suspension culture overnight at 37°C and 225 rpm bacterial orbital shaker in 50-200 mL LB Broth with appropriate antibiotics. Next, suspension culture was transferred to conical tubes and centrifuged at 4°C and 3750 rpm for 20 minutes. Macherey-Nagel (MN) Midi Prep kit was used to isolate plasmids from the pellets. For the plasmid DNAs obtained from commercial stab bacteria culture (distributed by Addgene), shipped bacteria were streaked onto LB agar plates to generate single colonies. Following steps are the same as mentioned above.

2.3 Virus production

To begin, HEK 293T cells cultured in D10(10% Fetal Bovine Serum, 1% Pen/Strep in DMEM High Glucose) were seeded to 10 cm plates at a density of 2x10^6 per plate. Next day, transfection was performed with 2 viral packaging plasmids and the plasmid of interest (250 ng of envelope protein encoding plasmid (VSV-G) 2250 ng Gag-Pol (pUMVC was used for retroviral plasmid constructs, psPAX2 was used for lentiviral plasmid constructs) and 2500 ng viral plasmid of interest using PEI as transfection reagent. For better activation, PEI was incubated 10 minutes at 70°C before each individual use. Plasmids and PEI were mixed with basal DMEM in separate tubes. For further PEI activation, PEI was incubated with DMEM at 5 minutes at room temperature. Then, plasmid mix, and PEI tubes were combined and incubated for 30 minutes. Next, combined mix was added to HEK293T cell culture medium in a dropwise manner to avoid detachment of cells. Supernatants of culture were collected at 48h and 72 h. Collection mix then were filtered with 0.45 um filters to clean any HEK debris. For supernatant virus production, filtered medium was aliquoted and stored at -80C. For concentrated virus production, 50% PEG8000 was added to the filtered medium at a ratio of 1:4. After 16 hours, tubes were centrifuged at 4°C and pellets were resuspended using cold PBS at a concentration of 100x and stored at -80°C.

2.4 Fibroblast viral infection

Fibroblast cells were counted and seeded at a density of 1x10^5 cells per a well of 6 well plate. After 24 hours, cells were infected with a 1 ml of supernatant virus with the addition of 0.5 mL D10 and protamine sulfate with final concentration of 8µg/mL. 16 hours post-infection, the same virus infection procedure was repeated. Next day, antibiotic selection was started by adding a medium with appropriate antibiotics (puromycin (1 µg/mL), blasticidin (7µg/mL), hygromycin (50 µg/mL))).

2.5 Protein extraction

Cells pellets were resuspended with RIPA Lysis Buffer (EcoTech, cat. RIPA-100) supplemented with 1 mM PMSF, 1X protease inhibitor. Resuspended cells were incubated in ice for 30 minutes with vortexing at every 10 minutes. Next, the cells were centrifuged at 13,000 rpm for 10 minutes at 4°C. Supernatant were transferred to the new

eppendorf tube. To quantify the concentration of the proteins in solution, Pierce™ BCA Protein Assay Kit (Thermo Fisher Scientific, cat. # 23225) was used.

2.6 Western blotting

First, 50 to 70 µg of lysate was mixed with a 4X Laemmli buffer (Bio-Rad,cat. #1610747) supplemented with β-mercaptoethanol (Bio-Rad,cat. #1610710) and then was boiled at 95°C for 15 minutes. Then, boiled samples and protein markers (Bio-Rad, cat. # 161-0374) were loaded into pre-cast SDS-PAGE gels (Bio-Rad, cat. # 456-1084). Next, gel electrophoresis for protein separation was performed using power supplies that apply 90 to100 volts. Separated proteins were transferred onto PVDF membrane (Bio-Rad, cat. # 1620177) using Bio-Rad trans-blot turbo transfer system. Then, membranes with transferred proteins were blocked by incubating with 5% milk solution at room temperature for 1 hour. Membranes were incubated with anti-USP22, anti-MENIN, anti-H3 Total antibodies diluted 1:500, 1:1000 and 1:1000 respectively in milk powder solution overnight at 4°C. Next day, the membranes were washed with TBS-T (Elabscience, cat. E-BC-R335) for 15 minutes 3 times. Then, membranes were incubated with secondary antibodies (Abcam, cat. #ab97051) with 1:5000 dilution for 1 hour at room temperature. Membranes were washed with TBS-T again three times for 15 minutes. Finally, membranes were incubated with Pierce™ ECL Western Blotting Substrate (cat. #32106) or SuperSignal™ West Femto Maximum Sensitivity Substrate (cat. #34094) then membranes were imaged using Odyssey Imaging System (LICOR Biosciences).

2.7 Immunofluorescence staining and imaging

Before immunofluorescent staining, cells were fixated using 4% paraformaldehyde (diluted in PBS, pH adjusted to 7.4). Following fixation, cells were washed with PBS three times for 5 minutes. Then, permeabilization was performed on cells using PBS supplemented with Triton X-100 (0.1%) for 10 minutes. Cells were again washed with PBS three times. The samples were then blocked using a blocking buffer (PBS containing 1% bovine serum albumin (BSA), 5% goat serum) at room temperature for 30 minutes. Then, primary antibodies were diluted using the ratios provided by the manufacturer. Anti-TRA-1-60(BioLegend cat. #330610), Anti-KLF17(Atlas, HPA024629), Anti-OCT4 (Abcam, cat. #ab19857), Anti-TRA 1-81 (BD Pharmingen cat# 560174) and Anti-SSEA4

(BD Pharmingen, cat# 560218) were used with concentrations of 1:250,1:250,1:1000,1:500,1:250 respectively. Next day, the cells were washed with PBS three times. Cells were incubated with Secondary antibodies diluted in a blocking buffer for 1 hr at room temperature. Then, cells were washed with PBS three times for 5 minutes each. Finally, DAPI staining (1µg/mL in PBS) was performed, and imaging was done using Cytation 5 (BioTek).

2.8 TRA 1-60 staining

To quantify the colony numbers at the end of reprogramming or percent area covered by colonies, TRA 1-60 immunostaining was used. PFA-fixed cells were washed with PBS twice and incubated with biotin-conjugated-anti-TRA 1-60 primary antibody (BioLegend 330604) diluted at the ratio of 1:250 in the staining solution containing 3% FBS, 0.3% Triton-X-100 in PBS overnight at 4°C.Next day, primary antibody solution was discarded, and cell were washed with PBS twice. Then, cells were incubated at room temperature for 1 hour with secondary antibodies that contain streptavidin and horseradish peroxidase (BioLegend 405210) diluted in staining solution at a ratio of 1:500. After that, DAB Mix was prepared by adding 0.1% 3,3'-diaminobenzidine, 0.05% nickel ammonium sulfate and 0.015% hydrogen peroxide. DAB mixtures were added to each well and brown spots were developed immediately around TRA 1-60 positive colonies. 20 minutes after DAB incubation, cells were washed with PBS twice and heavy cream was added to generate white background contrasting the developed stains. Plates were then scanned in the JPEG format with 600 dpi resolution. ImageJ software was used to analyze scanned images.

2.9 RNA isolation and cDNA conversion

For RNA Isolation cells were detached from plates and pelleted. Then, to extract total RNA from cells, a Nucleospin RNA kit (Macherey Nagel) was used according to manufacturer instructions. Isolated RNAs were measured using Thermo Scientific™ NanoDrop™ 2000/2000c Spectrophotometers. To prepare cDNA from extracted RNAs, from each sample, a mix that has volume up to 16 µL containing 500 ng total RNA, 2.5 µL of 2.5 mM dNTPs, 1µL of 50µM random hexamers were prepared. Mixture was heated at 65 °C for 5 minutes by using Bio-Rad T100 Thermal Cycler and then quickly put on ice for 5 minutes. Then, the second solution was prepared by mixing 5 µL 5X First

Strand Buffer, 2µL of 0.1M DTT, and 0.5 µL Rnasin. Second solution was added to each tube and incubated at room temperature for 10 minutes. After that, 1µL of MMLV RT was added to tubes and incubated at 37°C for 1 hour to catalyze reverse transcriptase reaction and 70 °C for 15 minutes to inactivate the enzyme. Reaction is diluted to 1:4 after incubation.

2.10 RT-qPCR

Light Cycler 480 SYBR Green I Master PCR Mix (Roche Life Sciences, cat. # 04707516001) is used for qPCR Reaction. cDNAs from each sample were mixed with appropriate primer sets (reverse and forward) and PCR Mix. Then, using Light Cycler® 480 Instrument II with the settings 40 cycles of 30 seconds at 95 °C, 30 seconds at 60 °C and 30 seconds at 72 °C. Endogenous GAPDH expression was used for all normalizations. Quantifications of relative expression of genes were calculated using the formula $2^{(Ct - Cc)}$ where Ct represents the main threshold cycle for genes and Cc represents the mean threshold cycle for calibrator.

Table 2.3. List of primers used for RT-qPCR

GAPDH Forward	CTCCTGCACCACCAACTGCT
GAPDH Reverse	GGGCCATCCACAGTCTTCTG
DNMT3L Forward	CAGTGCCTGCTCCTTATGGCT
DNMT3L Reverse	TGAACAAGGAAGACCTGGACG
LIN28 Forward	TGCGGGCATCTGTAAGTGG
LIN28 Reverse	GGAACCCTTCCATGTGCAG
GDF3 Forward	TTGTGTTGCGGTCAGTCCC
GDF3R Reverse	GGGGTTGTCATTCCAATCCTTAG
ALPPL2 Forward	TACCCAGATGACTACAGCCAA
ALPPL2 Reverse	TCGGTGGATCTCGTATTTCATGT
SOX2 Forward	AGCTACAGCATGATGCAGGA
SOX2 Reverse	GGTCATGGAGTTGTACTGCA
ARGFX Forward	CCGGAGTCAACAGTAAAGGTTTG
ARGFX Reverse	GGTGGGCACATTCTTCTTGGA
TFCP2L1 Forward	TCCTTCTTTAGAGGAGAAGC
TFCP2L1 Reverse	ACCAACGTTGACTGTAATTC
TFAP2C Forward	ACGAAATGAGATGGCAGCTAGGAAGA
TFAP2C Reverse	TGTCCGGTCTTGGCTGAGAAGTTC
DPPA5 Forward	TGCTGAAAGCCATTTTCG
DPPA5 Reverse	GAGCTTGTACAAATAGGAGC
KLF17 Forward	AGCAAGAGATGACGATTTTC
KLF17 Reverse	GTGGGACATTATTGGGATTC

OCT4 Forward	CCTCACTTCACTGCACTGTA
OCT4 Reverse	CAGGTTTTCTTTCCCTACGT
KLF4 Forward	TCTCAAGGCACACCTGCGAA
KLF4 Reverse	TAGTGCCTGGTCAGTTCATC
MYC Forward	ACTATGACCTCGACTACGACTC
MYC Reverse	TCGTCGCAGTAGAAATACGGC
DUSP6 Forward	GAAATGGCGATCAGCAAGACG
DUSP6 Reverse	CGACGACTCGTATAGCTCCTG
OTX2 Forward	CAAAGTGAGACCTGCCAAAAAGA
OTX2 Reverse	TGGACAAGGGATCTGACAGTG
CD24 Forward	ACCCACGCAGATTTATTCCA
CD24 Reverse	ACCACGAAGAGACTGGCTGT
POSTN-Forward	TAA GTT TGT TCG TGG TAG CAC C
POSTN-Reverse	GTG TGG GTC CTT CAG TTT TGA TA
FOXC2- Forward	CGA AGC TGA AGT TGG TAG GC
FOXC2- Reverse	GGT AGC AAC GTG CTG ACT GA
COL1A2 - Forward	GGCCCTCAAGGTTTCCAAGG
COL1A2 - Reverse	CACCCTGTGGTCCAACAACTC

2.11 Human primed reprogramming

dH1f cells were grown in fibroblast medium (DMEM,10% fetal bovine serum,1%Pen/Strep) and seeded at a density of 50.000 cells per well of 12-well plate.

Next day cells are transduced with O2S and K2M viruses with the total volume of 700 µL per well. Media is replenished with D10 next day and every two days.7 day after OSKM transduction, cells are detached with trypsin-edta incubation and 1:8 of them are passaged onto mitomycin-C treated MEFs (2 million MEFs per plate). Medium changed to homemade hES (20%KOSR, 1%PS, 1%NEAA, 0,1µg/ml FGF2 0.1% B-mercaptoethanol in the DMEM/F12 base medium) the next day and every two days. At day 15, cells are fixed using 4% PFA.

2.12 Human naïve reprogramming

dH1f cells grown in fibroblast medium (DMEM,10% fetal bovine serum) were seeded at a density of 50.000 cells per well of 12-well plate. Next day cells are transduced with O2S and K2M viruses with the total volume of 700 µL per well. Media is replenished with D10 next day and every two days.7 day after OSKM transduction, cells are detached with trypsin-edta incubation and 1:8 of them are passaged onto mitomycin-C treated MEFs (2 million MEFs per plate). On day 8 medium is replenished with D10 to give cells recovery before changing to naive conditions. On day 9, Media is switched to PGXL that prepared using base media that consist of DMEM/F12 and Neurobasal with the ratio of 1:1 which is supplemented with 1% Pen-Strep (Biowest), 1% GlutaMAX (Gibco), 1% N2 supplement, 2% B27 supplement, 10 ng/mL hLIF, 2 µM XAV939, 2 µM Gö6983, 1 µM PD0325901, 1.2 µM Y27632, (Guo et al., 2017) Then, media is replenished every day. At day 14 cells are fixated using 4% PFA.

2.13 Primed to naïve conversion

To convert primed pluripotent stem cells to naive pluripotent stem cells, HENSM-ACT condition is used. Primed pluripotent stem cells were seeded either on iMEFs (1M per plate) or 1% Geltrex coated plates in either E8 medium or homemade mTesr. Following day, media is switched to HENSM-ACT that prepared using base media that consist of DMEM/F12 and Neurobasal with the ratio of 1:1 which is supplemented with 1% Pen-Strep (Biowest), 1% GlutaMAX (Gibco), 1% NEAA, 1 mM sodium pyruvate, 1% N2 supplement, 2% B27 supplement, 50 µg/mL L-ascorbic acid 2-phosphate magnesium salt, 0.2% Geltrex, 20 ng/mL hLIF, 2 µM XAV939, 2 µM Gö6983, 1.2 µM PD0325901, 1.2 µM CGP77675, 1.2 µM Y27632, 0.8 µM BIRB796, 10 ng/mL Activin A. For Passaging, cells were first washed with PBS, then incubated with TrypLE(0.8x) for 3 minutes at

37°C. TrypLE is inactivated using serum containing media, and cell were collected to tube. After that, cells were centrifuged at 1.0 rpm for 3.5 minutes. Supernatant is aspirated and cell pellets are resuspended with HENSM-ACT supplemented with 10µM Y-27632. According to their confluence, cells were split with a ratio of 1:2 to 1:4 every 3-4 days.

2.14 Teratoma Formation Assay

To functionally characterize the iPSCs, teratoma formation assay was performed. iPSCs were resuspended in serum-containing media supplemented with Geltrex, followed by intramuscular injection into immunodeficient SCID Mice. Approximately 2 months post-injection, mice were sacrificed and teratomas were collected. H&E staining was performed to identify structures associated with three germ layers.

This study was conducted following the ethical guidelines for animal research approved by the HADYEK under the protocol code 2021.HADYEK.034.

2.15 Statistical analysis

T-test and one-way Anova tests are used for statistical analysis. Prism-10 GraphPad software is used for all tests and figure constructions.

CHAPTER 3:

RESULTS

3.1 USP22 is a barrier to reprogramming independent of its ubiquitinate function

To test the hypothesis that knocking out USP22 is the main reason behind the increase in reprogramming efficiency, I conducted a rescue reprogramming experiment. First, I generated USP22 KO Cell Lines using guides specifically targeting USP22 genes cloned in LentiCrisprV2 plasmid which includes protein sequence for Cas9 protein. Two USP22 cDNA constructs were previously generated (Gürhan, 2023) as described: PAM mutant USP22 sequence was cloned into Flag-HA-USP22 (Addgene, #22575) overexpression plasmid. Also, a point mutant was introduced to PAM Mutant USP22 cDNA (Gürhan, 2023). Then using these two constructs, I generated the cell lines in both (non-targeting 1) NT1 and USP22 KO backgrounds. Western blot results clearly showed that I was able to successfully express USP22 protein in USP22 KO Cells).

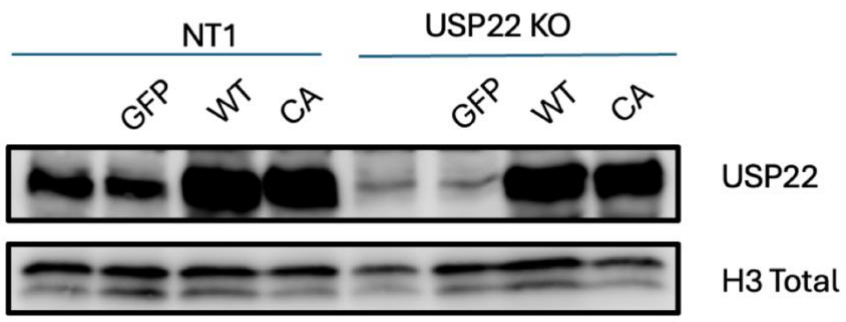

Figure 3.1. Western Blot showing USP22 protein levels after overexpressing USP22 in fibroblasts expressing non-targeting or USP22 targeting gRNAs. Histone H3 (H3 Total) antibody was used for loading control.

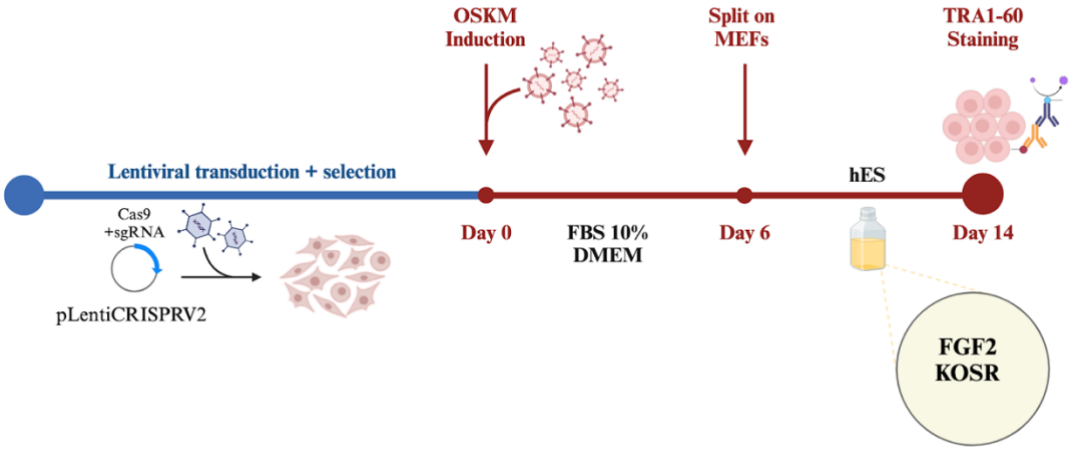

Figure 3.2. Schematics of Somatic Cell Reprogramming Protocol

TRA 1-60 Staining Result shows that loss of USP22 increases reprogramming efficiency by approximately 3-fold. Overexpression of wild type and catalytic mutant cDNA of USP22 (C185A) rescued the phenotype meaning that loss of USP22 is indeed the reason behind increase in reprogramming efficiency and its repressive effect to reprogramming is independent of its ubiquitinate activity.

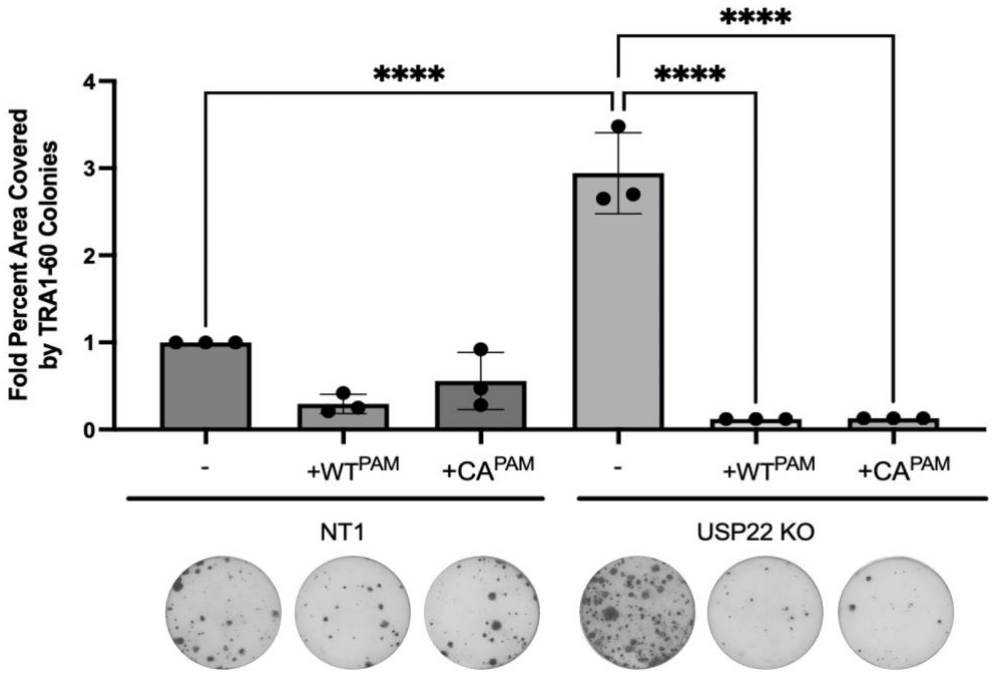

Figure 3.3. Fold change in percent area covered by TRA 1-60 positive colonies at the end of reprogramming. Error bars indicate the error of mean. n=3, independent experiments were performed. **** stands for $p \leq 0.0001$.

3.2 Knocking out (KO) USP22 enhances somatic cell reprogramming in primary adult fibroblast cell lines

To test if the increased reprogramming efficiency upon knocking-out UPS22 applies to a wide range of cell types, we utilized primary fibroblast cell lines that were collected from donors using punch-biopsy technique. These fibroblasts differ from dH1f fibroblast which has embryonic stem cell origin, and results in lower reprogramming efficiency. We generated two cell lines from each 4 donors including cells expressing non-targeting gRNAs and gRNAs targeting USP22. To check the expression levels of USP22, western blot analysis was performed. While cells expressing non-targeting gRNAs displayed signal for USP22 protein, cells expressing gRNAs targeting USP22 displayed no signal.

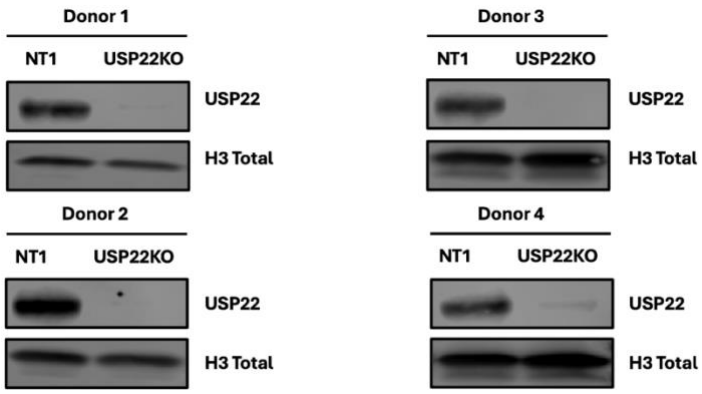

Figure 3.4. Western blot showing USP22 protein levels in fibroblasts expressing non-targeting or USP22 targeting gRNAs. Histone H3 (H3 Total) antibody was used for loading control.

Primary fibroblasts were reprogrammed using the protocol described before (Figure 3.2). Additionally, we also utilized two different primed culture conditions to show that the phenotype of knocking-out USP22 is independent of cell lines or culture conditions used. With the use of in-house prepared mTeSR medium and on geltrex, we were able to reprogram two of 4 donors, which resulted in 1.5-to-2-fold increase in terms of TRA 1-60 positive colony numbers. For fibroblasts reprogrammed using hES/MEF condition, three out of four donor fibroblasts were successfully reprogrammed which resulted in 1.5-to-3-fold increase. These results show that USP22 is a barrier to somatic cell

reprogramming independent of the cell's origin or culture conditions used during reprogramming.

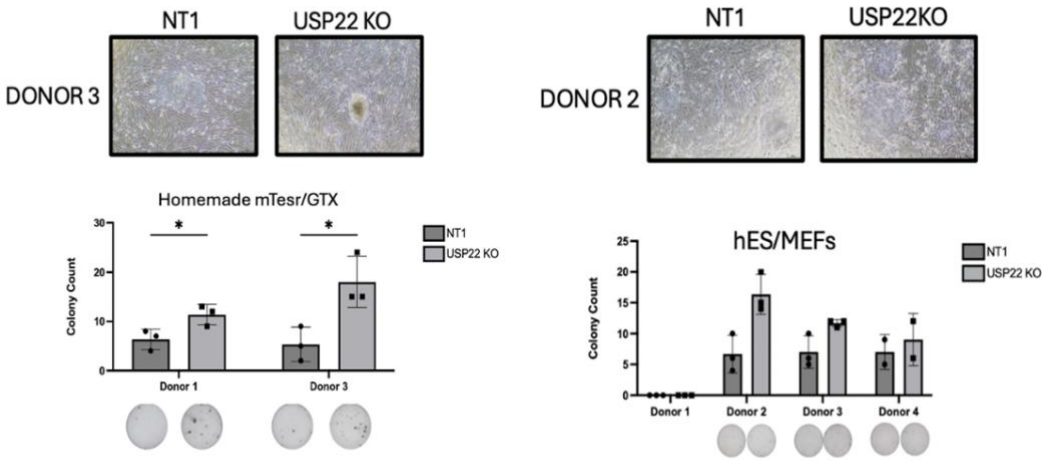

Figure 3.5. Representative phase-contrast images of iPSC colonies at the day of fixation and quantification of TRA 1-60 positive colony numbers for each donor in GTX/E7 (on left) or hES/MEFs (on right). Error bars indicate the error of mean. n=3 or n=2, independent experiments were performed. * Stand for $p<0.05$.

3.3 Time-course transcriptome analysis during primed reprogramming reveals that USP22 represses fibroblast specific gene network and enhances subset of naïve and general pluripotency genes.

Previous RNA-Seq Analysis (Gürhan et al., 2024) conducted on day 6 of reprogramming, had revealed that fibroblast-specific genes, such as *FN1*, *COL4A2*, *COL5A2*, *POSTN*, were downregulated in USP22 knockout (KO) cells compared to control cells. To validate the hypothesis that knocking out USP22 enhances reprogramming efficiency by repressing fibroblast-specific somatic gene networks, I performed a time-course RT-qPCR to analyze transcriptome at specific time points. I found that fibroblast-specific genes remained down regulated throughout reprogramming

including both under serum-containing culture conditions (prior to day 6) and serum-free primed pluripotency culture conditions (post day 6).

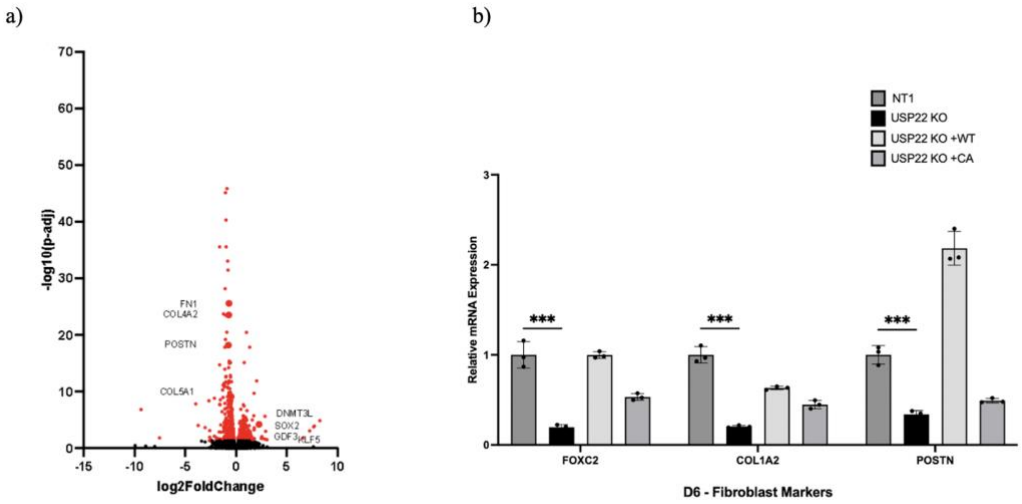

Figure 3.6. (a) Volcano Plot displaying differentially expressed genes at Day6 of reprogramming (Gürhan et al., 2024). (b) RT-qPCR results illustrate the relative mRNA expression levels of fibroblast-specific genes at Day 6. . Error bars indicate the error of mean. n=3, independent experiments were performed. *** stands for $p \leq 0.001$.

From Day 12, representing the late primed condition, fibroblast-specific genes such as *POSTN*, *FOXC2*, and *COL1A2* were downregulated by 2- to 10-fold compared to the control. Similarly, this phenotype was consistently observed at Day 9 (early primed condition) and Day 6. (Figures 3.6 and 3.7) These findings suggest that USP22 knockout enhances reprogramming efficiency by repressing fibroblast-specific genes throughout all phases of reprogramming (Figure 3.7).

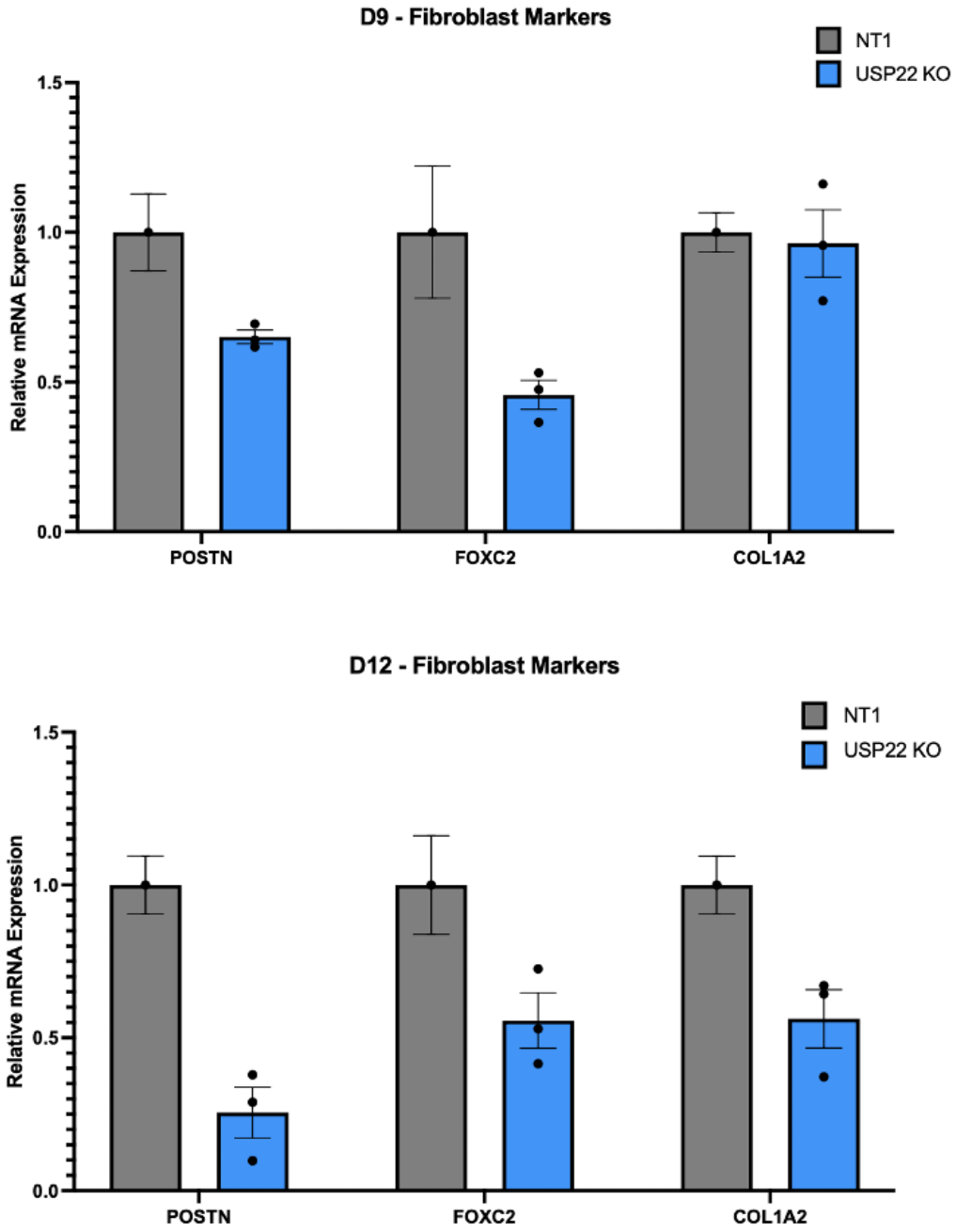

Figure 3.7. RT-qPCR results showing the relative mRNA expression levels of fibroblast-specific markers (POSTN, FOXC2 and COL1A2) on day 9 (early primed phase) and on day 12 (late primed phase) of reprogramming. Error bars indicate the error of mean. n=3, independent experiments were performed.

Another hypothesis generated from RNA-Sequencing analysis was that knocking out USP22 enhances reprogramming efficiency via upregulating specific pluripotency markers including DNMT3L, GDF3, SOX2, and LIN28A. To test whether this hypothesis applies across all phases of reprogramming, I analyzed the transcriptome using RT-qPCR at the previously mentioned time-points. I observed that DNMT3L, GDF3, SOX2 were consistently upregulated by 3- to 5- fold compared to control cells under serum-free primed pluripotency conditions, corresponding to Day 9 and Day 12 (Figure 3.8).

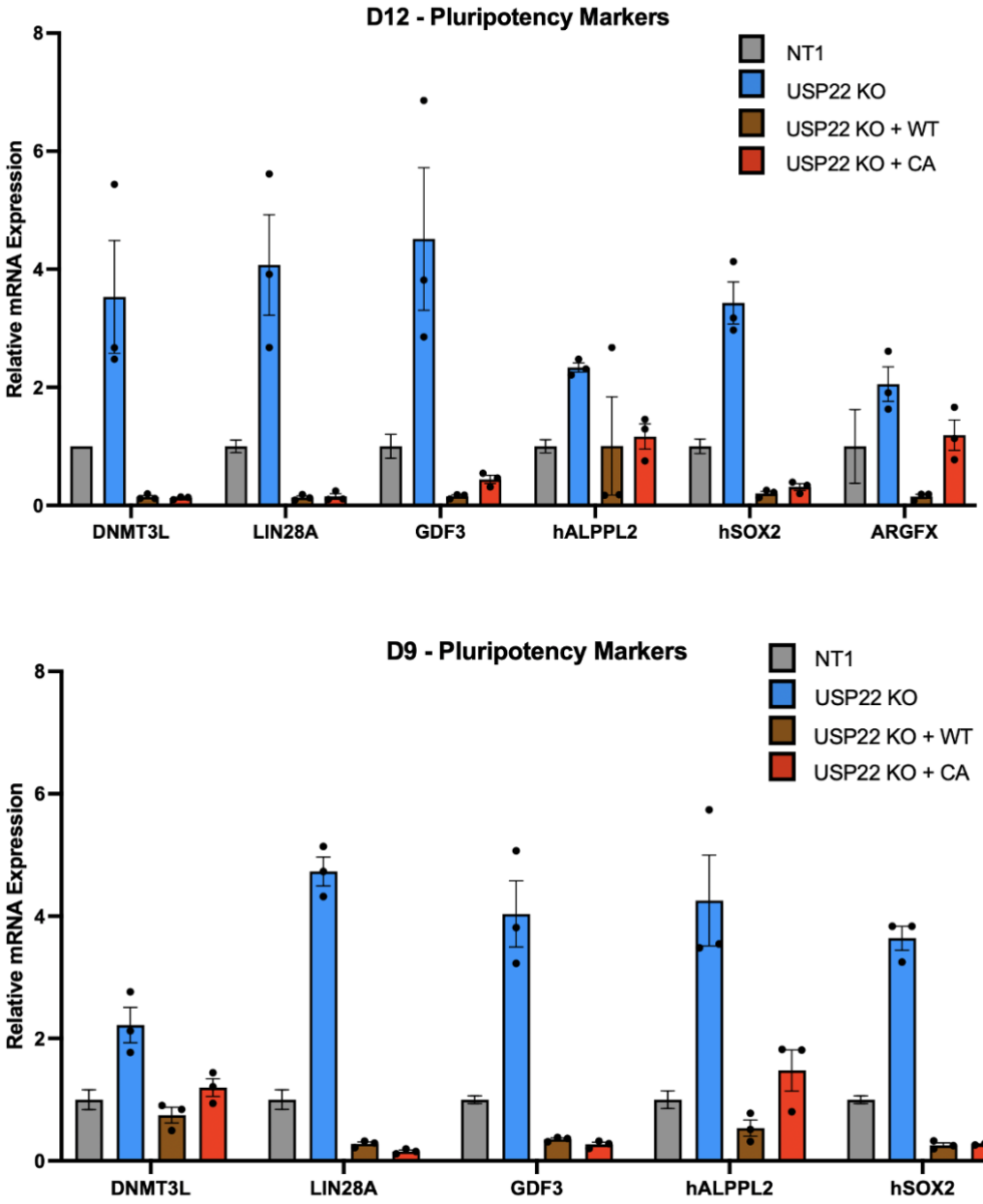

Figure 3.8. RT-qPCR results showing the relative mRNA expression levels of pluripotency markers (DNMT3L, GDF3, LIN28A, ALPPL2, ARGFX and SOX2) at Day 9(early primed phase) and at Day 12 (late primed phase) of Reprogramming, when compared USP22 KO to control. Error bars indicate the error of mean. n=3, independent experiments were performed.

To determine whether the upregulation of pluripotency genes also occurs during the serum-containing early phase of reprogramming, I applied the same approach to analyze day 3 and day 6 of reprogramming. I observed that even as early as at Day 3, DNMT3L, GDF3 and SOX2 exhibit 2-to 3- fold increase in expression levels compared to control, while LIN28A showed no such increase, meaning that apart from LIN28A, upregulation of pluripotency genes that we identified in RNA-Sequencing analysis extends to the earliest phases of reprogramming (Figure 3.9).

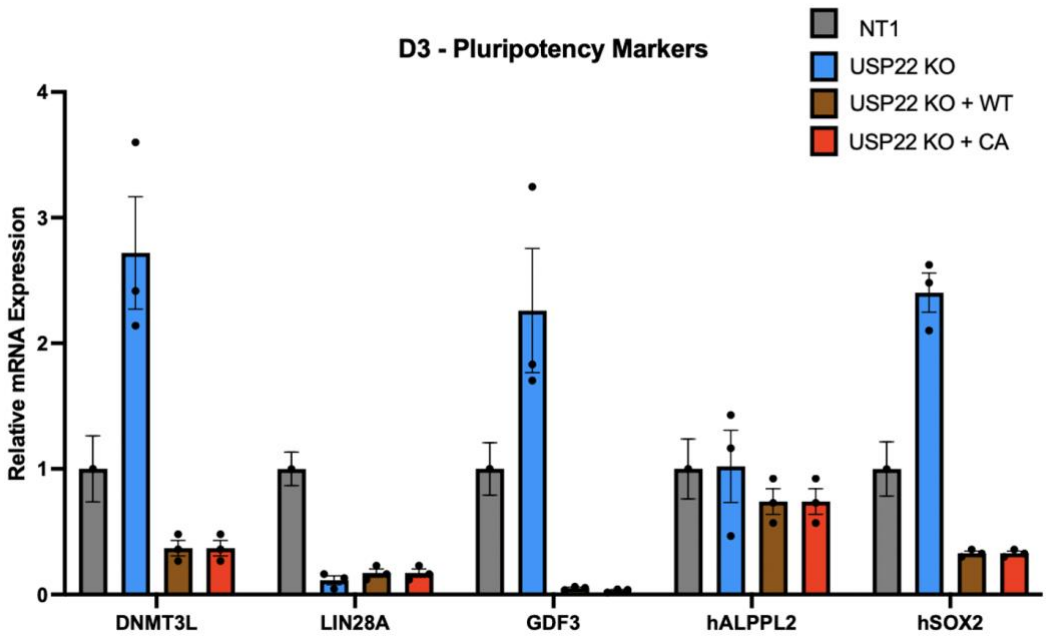

Figure 3.9. RT-qPCR results showing the relative mRNA expression levels of pluripotency genes (DNMT3L, GDF3, LIN28A, ALPPL2, and SOX2) at Day 3 (early serum-containing phase) of reprogramming. Error bars indicate the error of mean. n=3, independent experiments were performed.

Since *DNMT3L*, *GDF3* are genes that are known to be expressed higher in naive conditions, I hypothesized that knocking out USP22 might enhance the expression of other naive specific markers as well. Therefore, I added genes that are exclusively expressed in naive conditions including *ALLPL2* and *ARGFX* to our time-course transcriptome analysis. I observed up to 4- fold increase for ALPPL2 at Day 9, also up to 2-fold increase for ARGFX at Day 12(Figure 3.8). Seeing these robust upregulations in naive markers at different stages of reprogramming and knowing that naive markers are activated at late stages of reprogramming, I analyzed the naive marker at the time of fixation. Then, to see if naive marker upregulation is trending upwards throughout the reprogramming, we analyzed the naive specific gene expression levels at each time point and normalized the levels to Day 0 fibroblast expression levels. We observed that at the time of day 14, naive-specific markers TFAP2C and TFCP2L1 are upregulated up to 6-fold. Finally, when we normalized these expression levels to day 0 fibroblast expression levels, we observed that upregulation of naive specific genes is trending upwards as time progresses in reprogramming (Figure 3.10).

a)

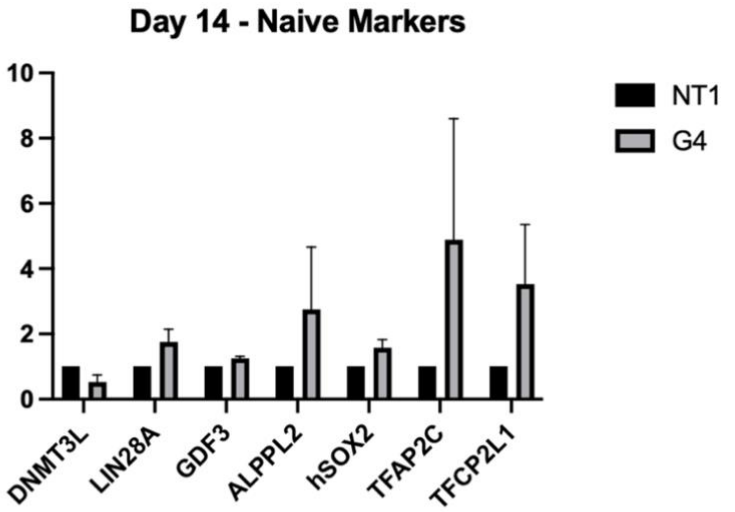

b)

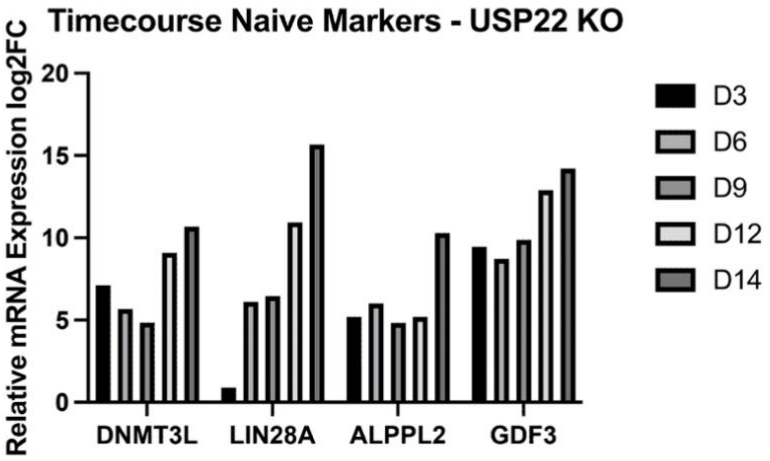

Figure 3.10. (a) RT-qPCR results showing the relative mRNA expression levels of pluripotency markers (DNMT3L, GDF3, LIN28A, ALPPL2, TFAP2C, TFCP2L1 and SOX2) at the end of reprogramming. (b) RT-qPCR results showing the relative mRNA expression levels of pluripotency markers at specific time points. Expression levels are normalized to pre-OSKM USP22 KO fibroblasts. Error bars indicate the error of mean. n=3, independent experiments were performed.

3.4 Knocking out (KO) USP22 enhances somatic cell reprogramming to naïve state pluripotency

To test the hypothesis that knocking out USP22 results in increased reprogramming efficiency at higher developmental potency, I designed and employed a modified version of our reprogramming protocol. Typically, OSKM transduced cells are transferred to serum-free naive conditions on Day 6. However, I observed our control group is not able to survive this drastic shift in culture conditions. To address this issue, I extended serum-based culture period to Day 8 to provide cells with additional time to recover from the stress of splitting. On Day 8, the cells were transitioned to naive culture conditions. Finally, on Day 14 cells were fixed for immunofluorescence (IF) staining (Figure 3.11).

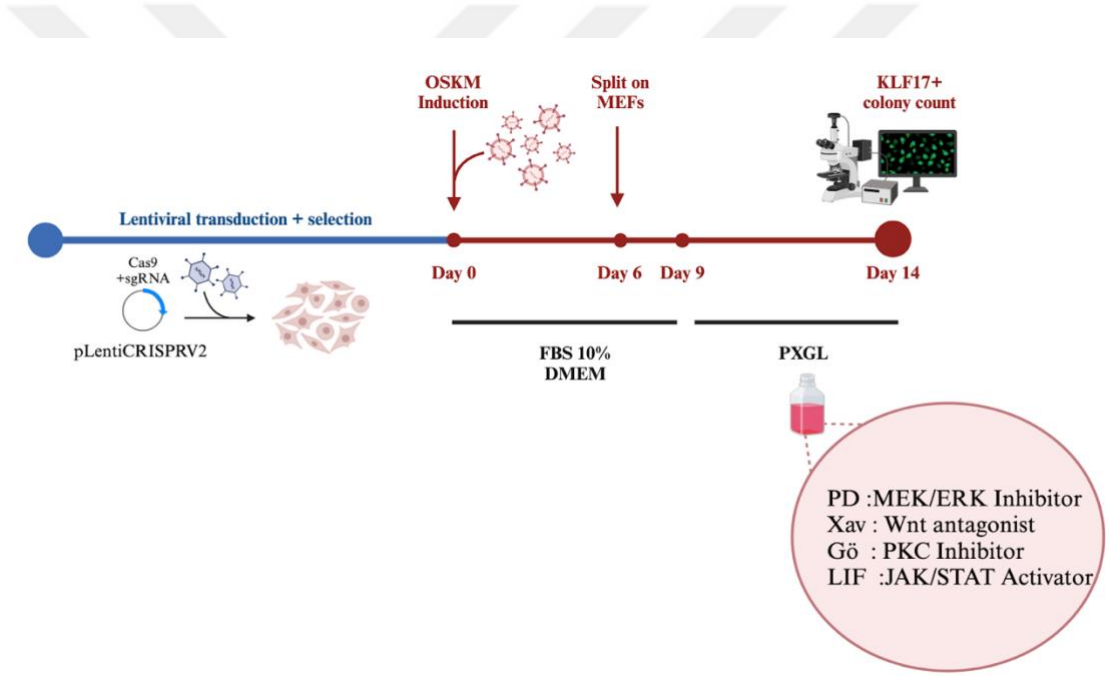

Figure 3.11. Schematics of Somatic Cell Reprogramming to Naïve Pluripotency Protocol.

To quantify induced pluripotent (iPSC) colonies, a TRA 1-60 antibody was selected. Since KLF17 is a specific marker protein for human naïve pluripotency state (Lea et al., 2021), to identify naive colonies within these TRA 1-60 positive colonies, KLF17 antibody was used. I defined colonies that were double positive for TRA 1-60 and KLF17 as naïve colonies. Using a high-content imaging microscope, I quantified both TRA 1-60 positive colonies and TRA 1-60/KLF17 double positive colonies. I observed an increase in the numbers of naive colonies (Figure 3.12).

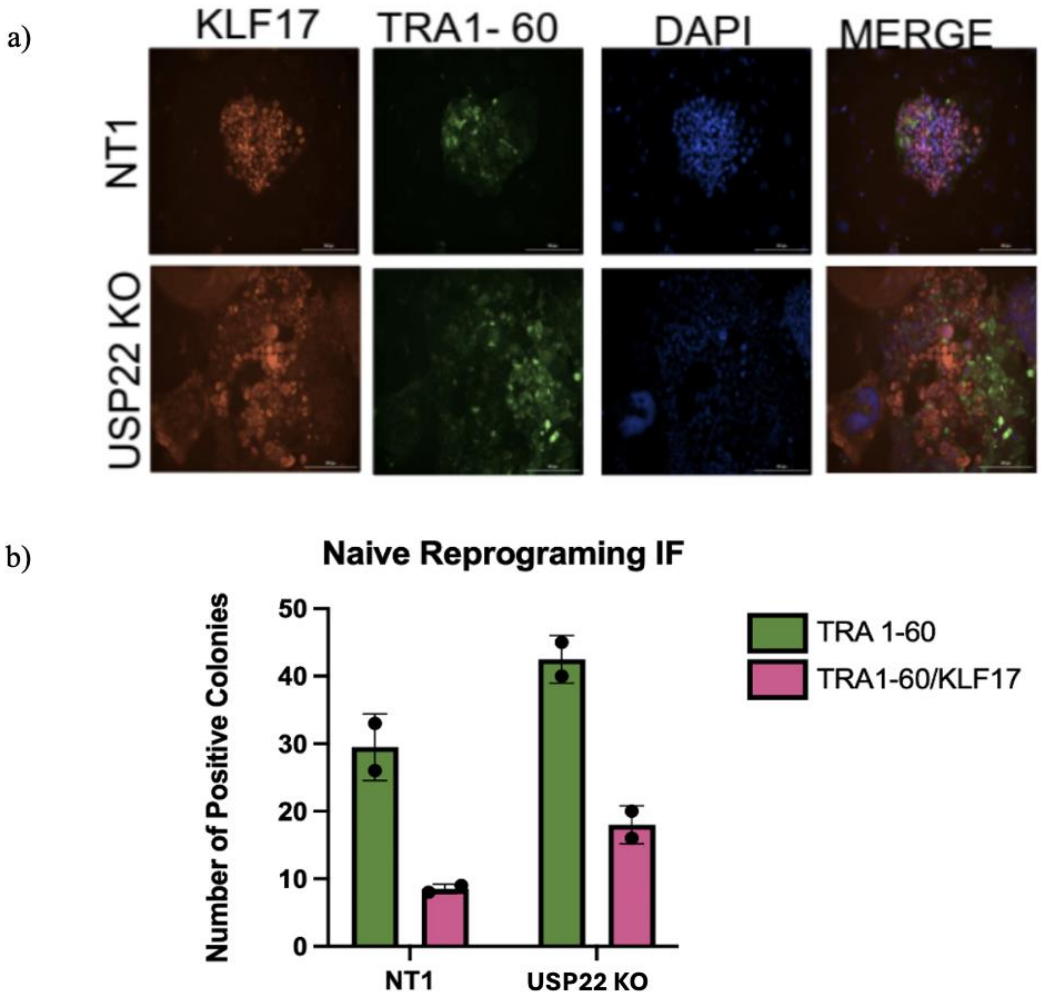

Figure 3.12. (a) Representative immunofluorescence (IF) Images displaying TRA 1-60/KLF17 double positive colonies. (b) Quantification of colonies positive for only TRA 1-60 and double positive for TRA 1-60/KLF17. Error bars indicate the error of mean. n=2, independent experiments were performed.

Although I observed robust KLF17 expression at the protein level, reprogramming cultures exhibit heterogeneous identity including KLF17 positive naive colonies, only TRA 1-60 positive primed colonies, and other partially reprogrammed cells. To test if USP22 KO cells generated authentic naïve cells, we transfer the USP22 KO cells into freshly coated MEFs plate in the same naive condition. Cells were passed every 3-4 days for a total of 4 passages and when cells reached approximately 70% confluency at passage 4, RNA was collected for gene expression analysis. I observed that USP22 KO cells

cultured under naive conditions displayed appropriate expression of naïve-specific marker genes alongside low expression of primed-specific marker genes indicating loss of traditional iPSC identity and acquisition of naive-like characteristics (Figure 3.13).

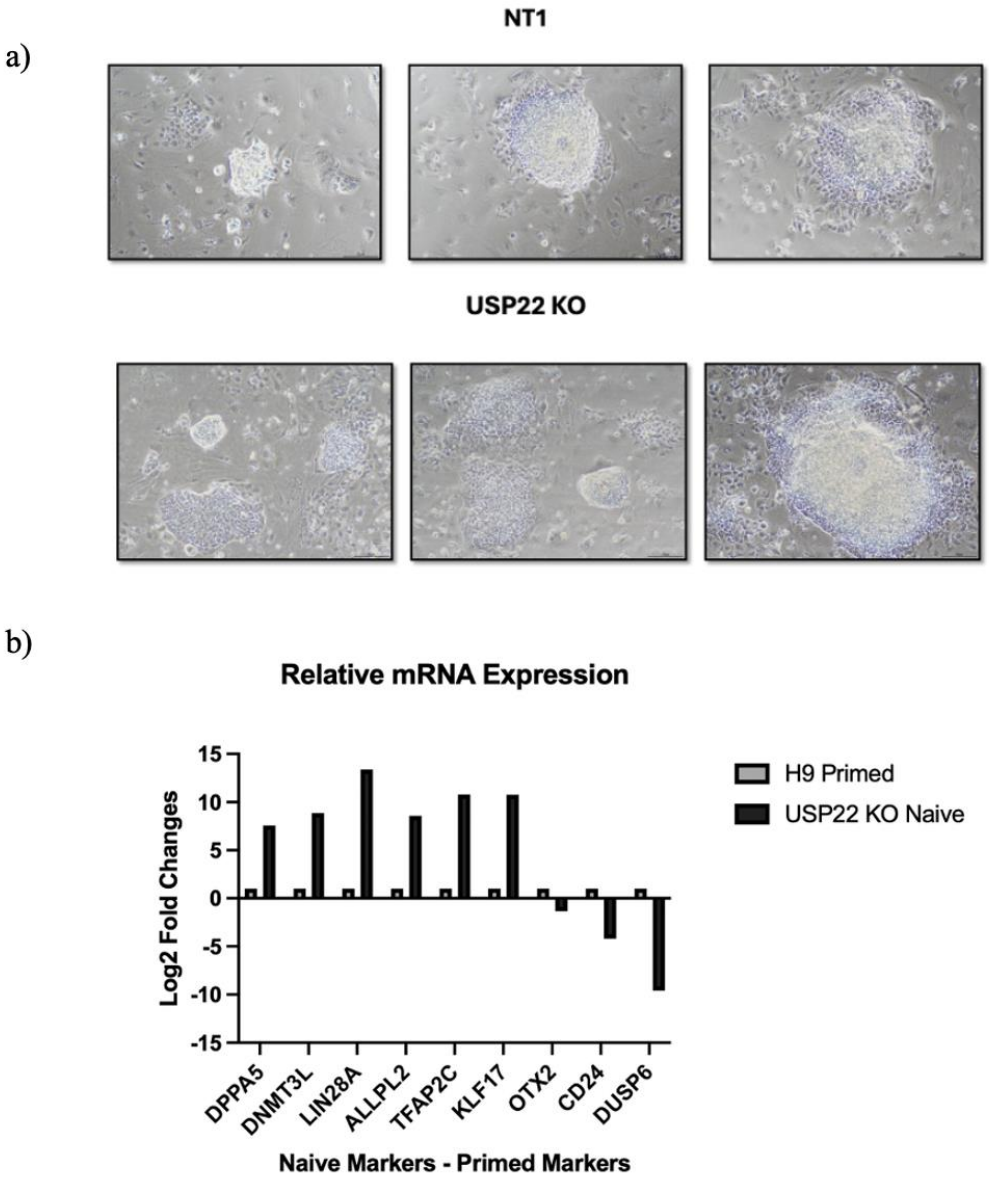

Figure 3.13. (a) Representative light contrast imaging of naïve reprogramming culture at the day of fixation showing colonies with distinct morphologies. (b) Relative mRNA Expressions of USP22 KO iPSC cultured in naïve conditions for 4 passages, normalized to H9 Primed.

3.5 USP22 loss upregulates a subset of naive pluripotency genes during primed to naive conversion

To test whether USP22 has a repressive effect within the pluripotency window, I performed primed to naive conversion using previously established HENSM-ACT culture conditions (Bayerl et al., 2021). I first seeded NT1 and USP22 KO Cells on MEFs or GTX with E8 medium. Next day, I switched the media to HENSM-ACT and passaged the cells every 3 days while collecting RNA at each passage. I analyzed naive gene expression profiles using RT-qPCR and observed that although some subset of naive markers such as DNMT3L and ALLPL2 were consistently induced higher compared to NT1 control, we did not observe such consistency for KLF17. These results suggest that USP22 may have a repressive effect in activating specific subsets of naive gene networks.

a)

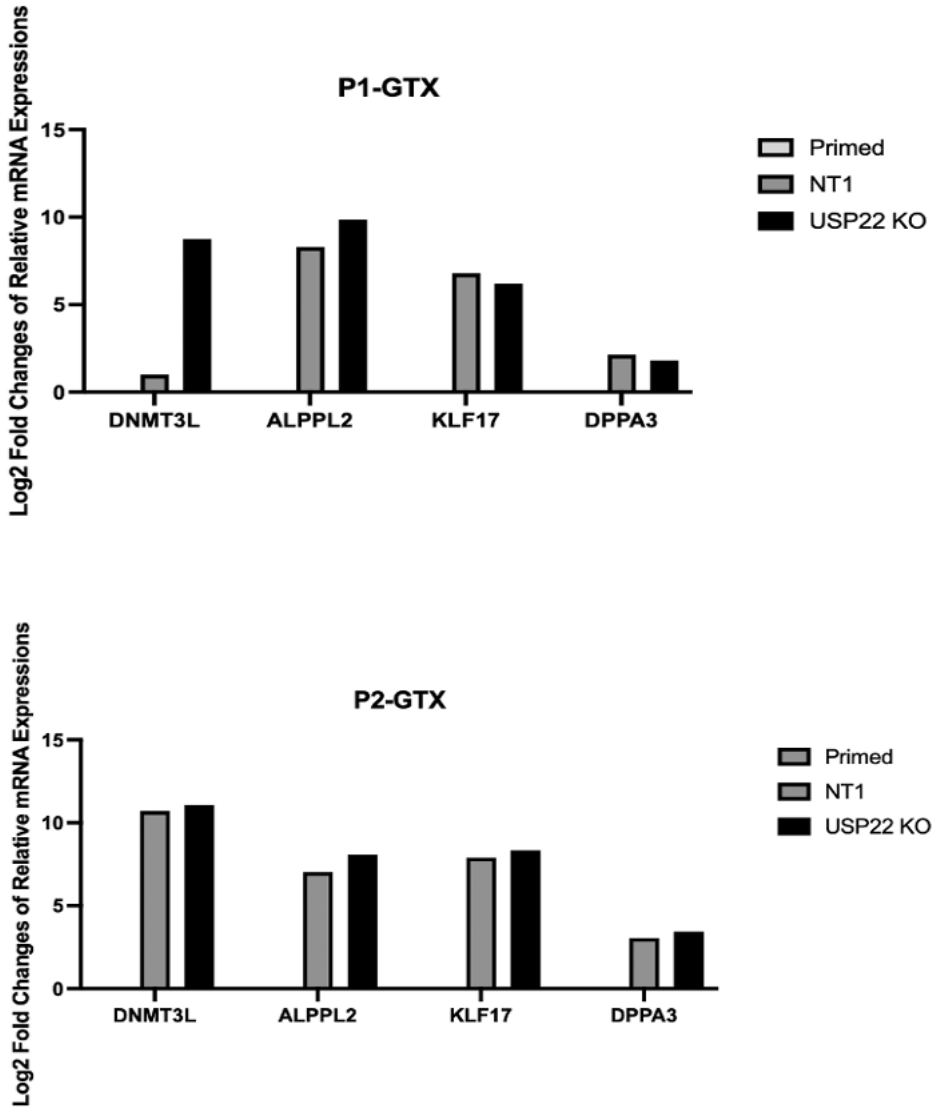
P1-GTX
Log2 Fold Changes of Relative mRNA Expressions
15
10
5
0
DNMT3L
ALPPL2
KLF17
DPPA3
Primed
NT1
USP22 KO
P2-GTX
Log2 Fold Changes of Relative mRNA Expressions
15
10
5
0
DNMT3L
ALPPL2
KLF17
DPPA3
Primed
NT1
USP22 KO

b)

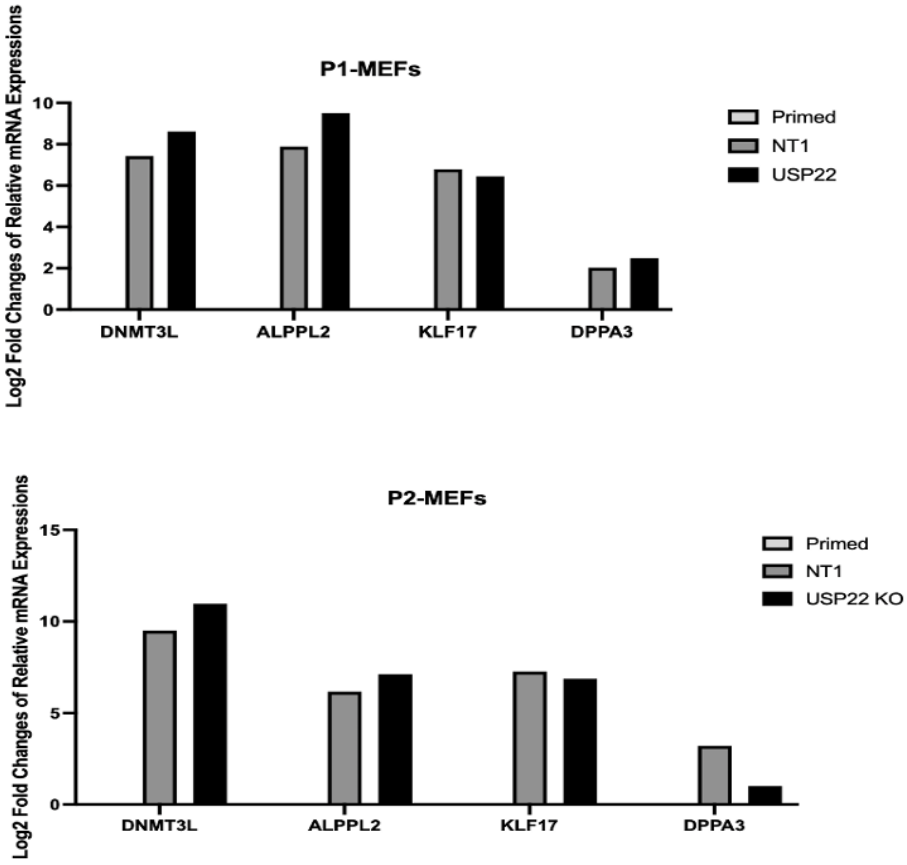

Figure 3.14. RT-qPCR results showing the relative mRNA expression levels of naive pluripotency genes (DNMT3L, ALPPL2, KLF17, DPPA3) at Day 3(P1) and Day 6 (P2) of naive conversion using feeder-free Geltrex (a) or MEFs feeder layer (b).

3.6 Loss of MENIN enhances reprogramming efficiency in primary fibroblast cell lines

To test if loss of MEN1 phenotype is applicable independent of cell line of choice. I generated MEN1 knockout from three primary fibroblast cell lines (Figure 3.15). Although we observed variance in terms of colony number fold change that differs among cell lines, MEN1 loss increased reprogramming efficiency by approximately 15 to 30-fold compared to control (Figure 3.16).

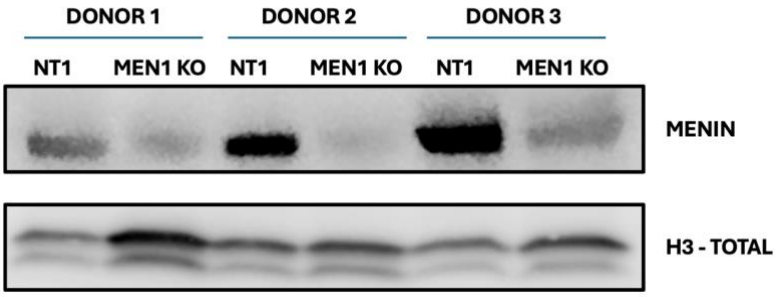

Figure 3.15. Western blot showing MENIN protein levels of fibroblasts expressing non-targeting gRNAs or MEN1 targeting gRNAs.

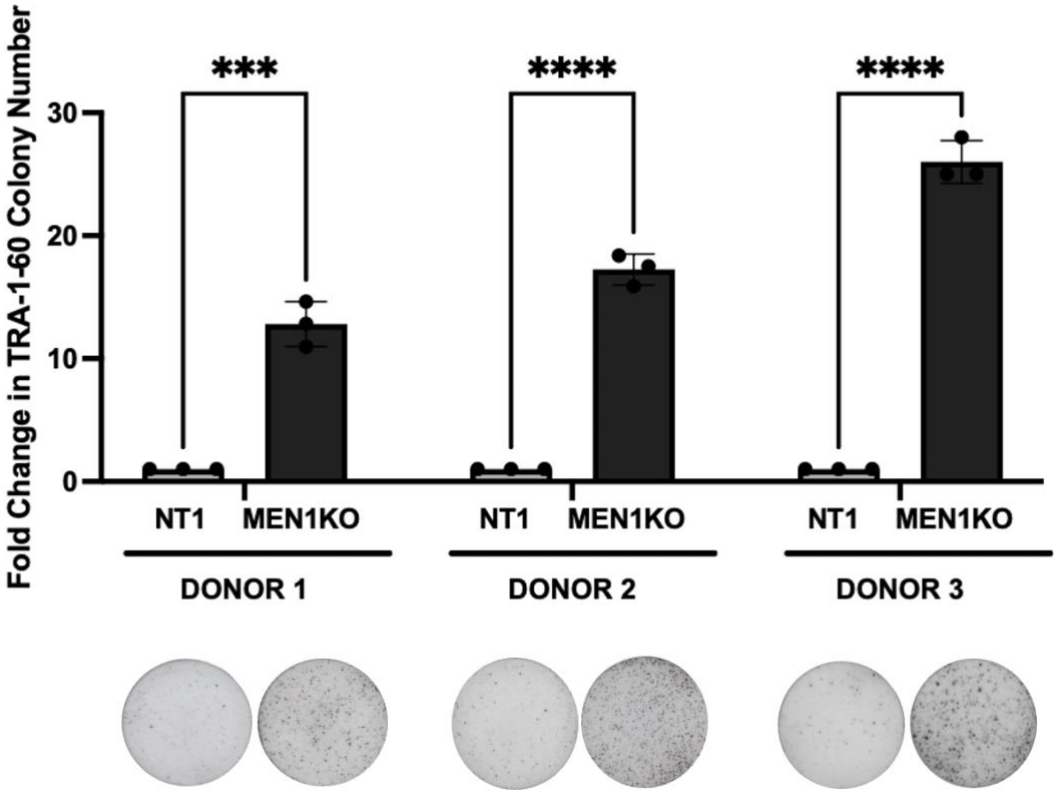

Figure 3.16. Fold change in TRA 1-60 positive Colony Number at the end of reprogramming upon knockout of MEN1 in three different primary fibroblast cell lines. Error bars indicate the error of mean. n=3, independent experiments were performed. *** stands for $p \leq 0.001$, **** stands for $p \leq 0.0001$.

3.7 MENIN is a barrier to reprogramming partially due to its ability to recognize H3K79me2

Recently MENIN was shown to recognize H3K79me2 through its H433 residue (Lin et al., 2023). To test if MENIN's repressive effect on somatic cell reprogramming is related to this specific chromatin reading ability, I generated H433A point mutant on PAM Mutant WT MEN1 sequence and transduced it to MEN1 KO Fibroblasts. Then, I checked MENIN levels via western blot which indicated stable expression of the H433A mutant (Figure 3.17).

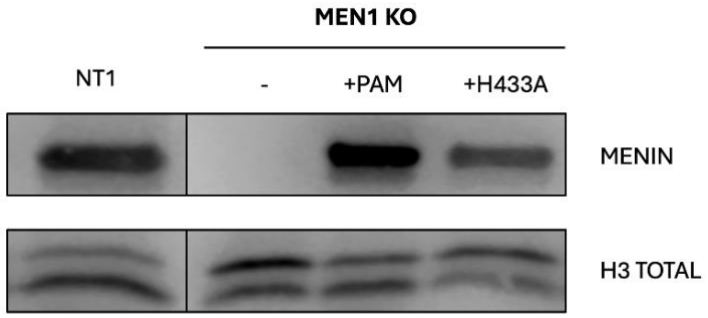

Figure 3.17. Western Blot showing MENIN protein levels after overexpressing MENIN in fibroblasts expressing non-targeting or MEN1 targeting gRNAs. Histone H3 (H3 Total) antibody was used for loading control.

Next, I reprogrammed the generated cell lines and observed that PAM mutant WT MENIN rescued the phenotype whereas H433A mutant MENIN partially rescued it (Figure 3.18). This finding suggests that MENIN's ability to repress reprogramming is partially related to its ability to recognize H3K79me2 chromatin mark.

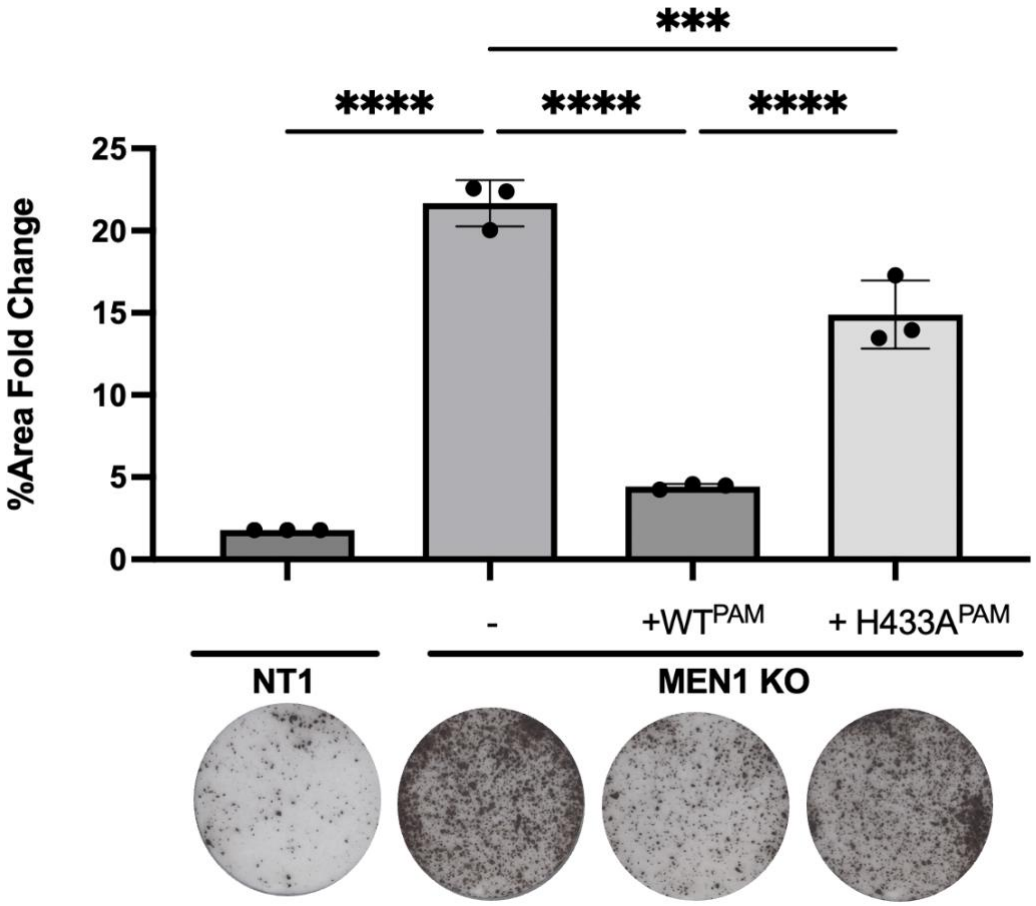

Figure 3.18. Fold change in percent area covered by TRA 1-60 positive colonies at the end of reprogramming. Error bars indicate the error of mean. n=3, independent experiments were performed. *** stands for p≤0.001, **** stands for p≤0.0001.

3.8 Time-course dox inducible MENIN rescues MEN1 loss phenotype

To investigate the which stages of reprogramming that *MEN1* Loss affects most, we designed a tet-on system where we cloned PAM Mutant WT MENIN cDNA into tet inducible expression plasmid (Addgene #84008). Then, MEN1 KO fibroblast are co-transduced with tet-inducible plasmids (GFP is also cloned for comparison control) and FUW-M2rtTA (Plasmid #20342) viruses under tet-free serum containing conditions. Western blotting was used to check expression of MENIN Protein (Figure 3.19). Next, generated fibroblast cell lines are reprogrammed using OSKM induction.

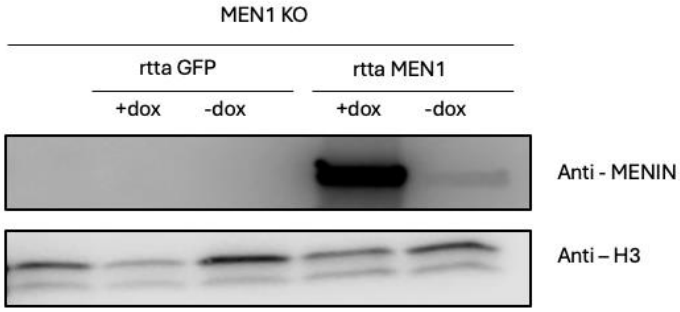

Figure 3.19. Western blot showing MENIN protein levels after co-transduction with FUW-M2rtTA and FUW-tetO-MCS (GFP or MEN1) in fibroblasts expressing MEN1 targeting gRNAs.

Reprogramming experiment is performed with four separate groups. First group received dox from Day 1 to Day 3, Second group received dox from Day 1 to Day 6, and third group received dox from Day 1 to Day 14 and last group received no dox after OSKM induction. When compared to GFP control, we observed a similar reduction in TRA-1-60 positive cells even in no dox group might mean that the tet-on system is leaky, and MENIN is expressed even in the absence of dox.

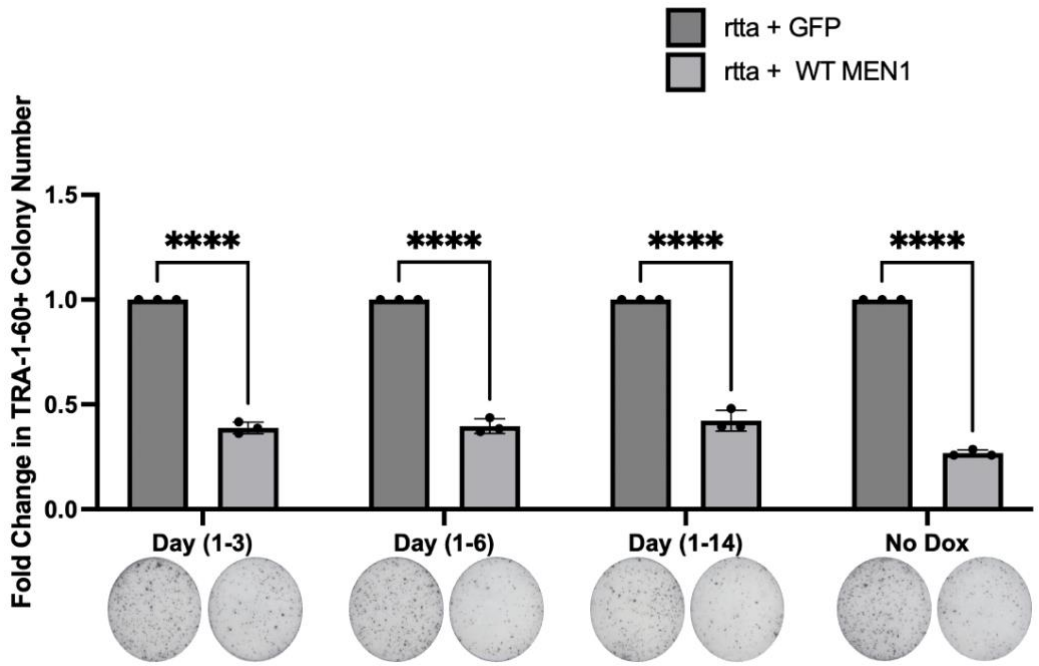

Figure 3.20. Fold change in TRA-1-60 positive colony number after Reprogramming. Error bars indicate the error of mean. n=3, independent experiments were performed. *** stands for p≤0.001, **** stands for p≤0.0001.

In addition, when we compared all groups to control (MEN1 KO + rtta-GFP, no dox), we observed that there is a slight reduction in TRA 1-60 positive cell count between 3 groups that might mean that MENIN's barrier function persists throughout the reprogramming.

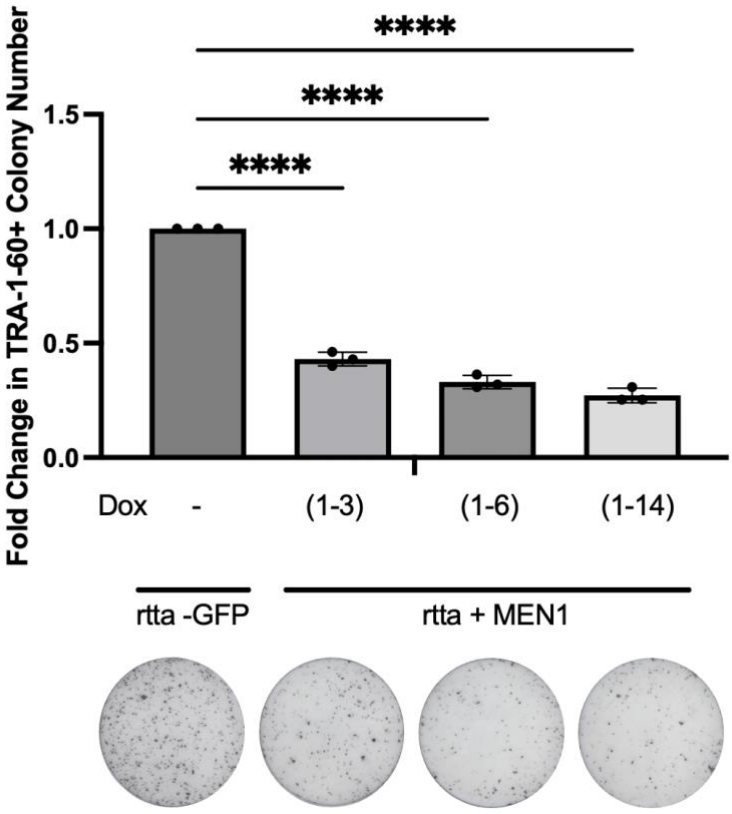

Figure 3.21. Fold change in TRA-1-60 positive colony number after Reprogramming. Error bars indicate the error of mean. n=3, independent experiments were performed. *** stands for p≤0.001, **** stands for p≤0.0001.

3.9 MENIN-MLL1 complex inhibition enhances reprogramming efficiency of primary fibroblast cell lines

Previously, it was shown that MLL1-MENIN inhibition through VTP50469 treatment increases reprogramming efficiency, and this enhancement is maximized via using the inhibitor for 14 days (Yılmaz, 2023). To test if increased reprogramming efficiency via MENIN-MLL1 inhibition is applicable independent from the cell line of choice, I reprogrammed three different primary fibroblast cell lines while treating them with VTP50469 compared to DMSO control. We observed up to a 12-fold increase in the TRA 1-60 positive colony number (Figure 3.22).

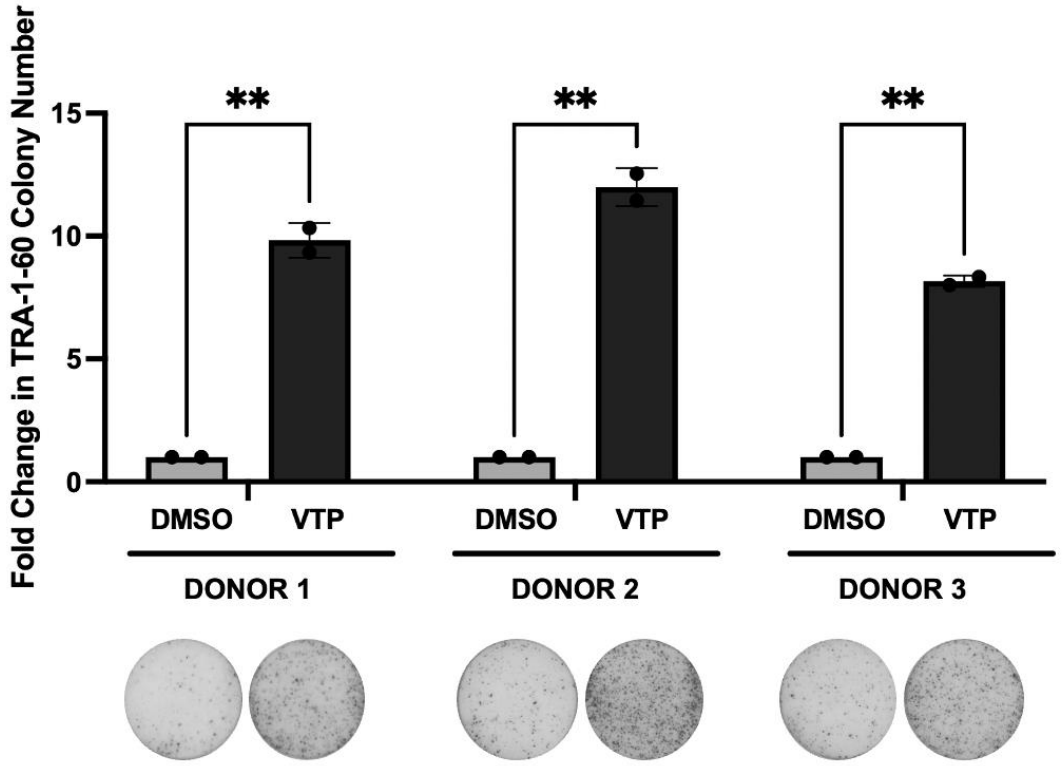

Figure 3.22. Fold change in TRA 1-60 positive Colony Number after treatment with 1 µM VTP50469. Error bars represent error of mean. n=2, independent experiments were conducted. ** stands for $p \leq 0.01$.

3.10 MENIN-MLL1 inhibition enhances 3-factor reprogramming and enables 2-factor reprogramming independent of culture conditions or viral vector of choice

Since c-MYC is an oncogene, it is preferable to reprogram somatic cells without overexpressing it. To determine whether VTP50469 supplementation also increases the reprogramming efficiency in the context of 3-factor reprogramming, I utilized individual pMIG-OCT4, pMIG-SOX2 and pMIG-KLF4 vectors and observed approximately 3-fold increase in the TRA-1-60 positive colony number indicating that VTP50469 also enhances reprogramming efficiency in the absence of the C-MYC proto-oncogene (Figure 3.23).

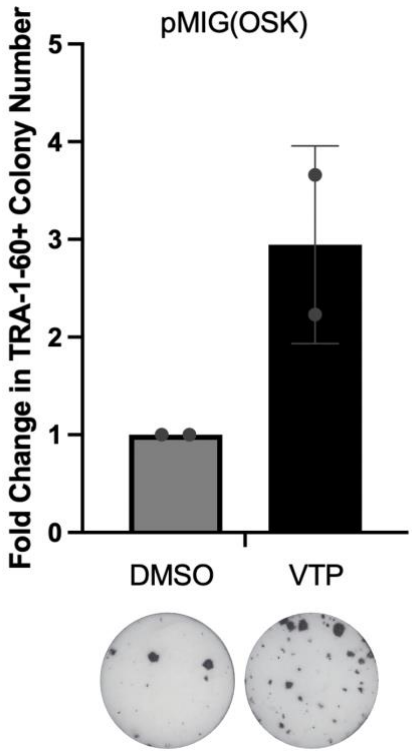

Figure 3.23. Fold change in TRA-1-60 positive colony number after OSK Reprogramming. Error bars represent error of mean. n=2 independent experiments were performed.

I next tested whether inhibiting MENIN-MLL1 complex enables dH1f cells to be reprogrammed using only the overexpression of OCT4 and SOX2 instead of using traditional approach that requires overexpressing all four Yamanaka Factors (OCT4, SOX2, KLF4 and c-MYC). To investigate this, I designed an experiment that utilized two

types of viral vectors: the lentiviral pSIN4 O2S and the retroviral pMIG-OCT4 and pMIG-SOX2. Then, for primed culture conditions, I employed both the hES/MEF combination and E7/GTX. While the control group was treated with DMSO, the experimental group was treated with VTP50469 (1uM final concentration) for 14 days, then at day 21, TRA 1-60-positive colonies were quantified. I observed that while there are only a small number of colonies in the DMSO-treated groups, VTP50469-supplemented groups produced 50 to 100 colonies (Figure 3.24). Therefore, I concluded that VTP50469 supplementation enables efficient 2-factor somatic cell reprogramming, reducing the reliance on all four Yamanaka Factors. Furthermore, the conclusion is applicable to various viral vector systems and primed culture conditions.

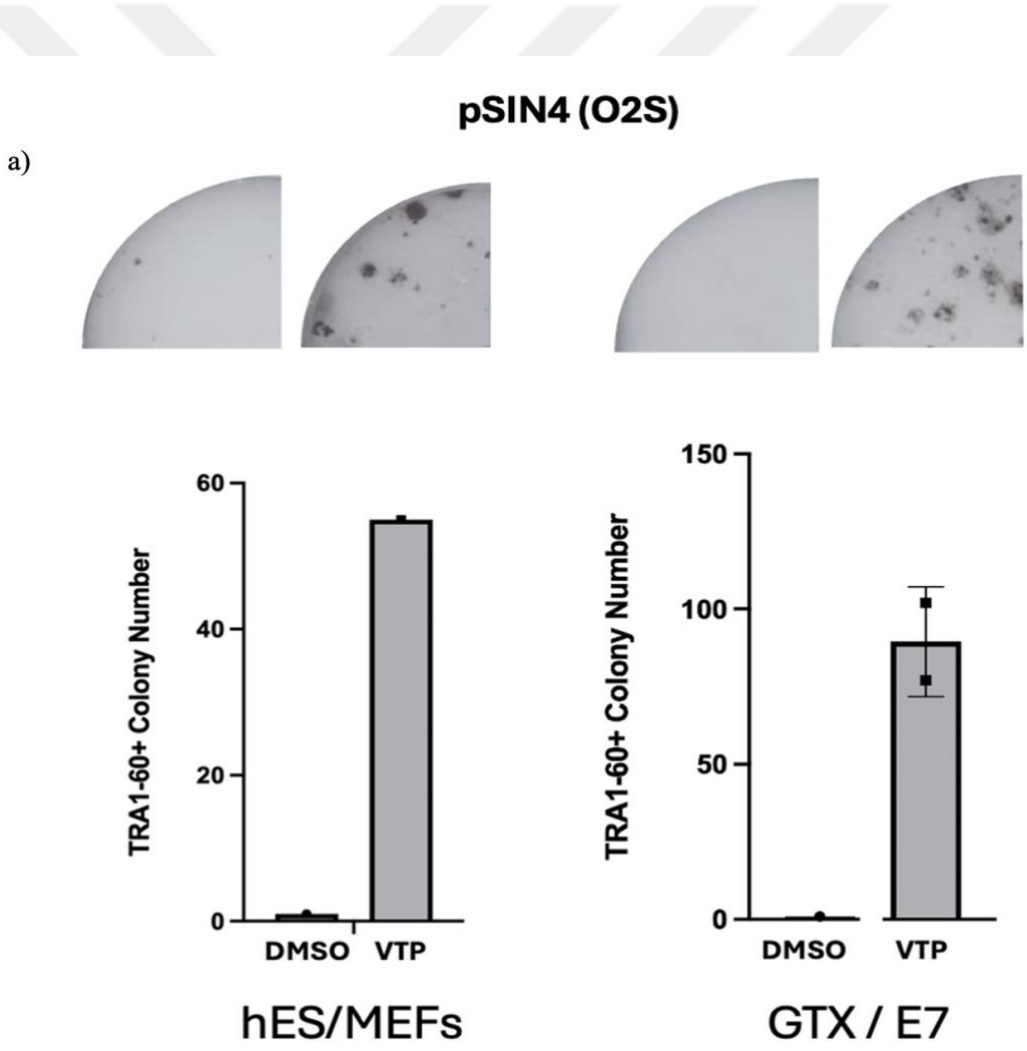

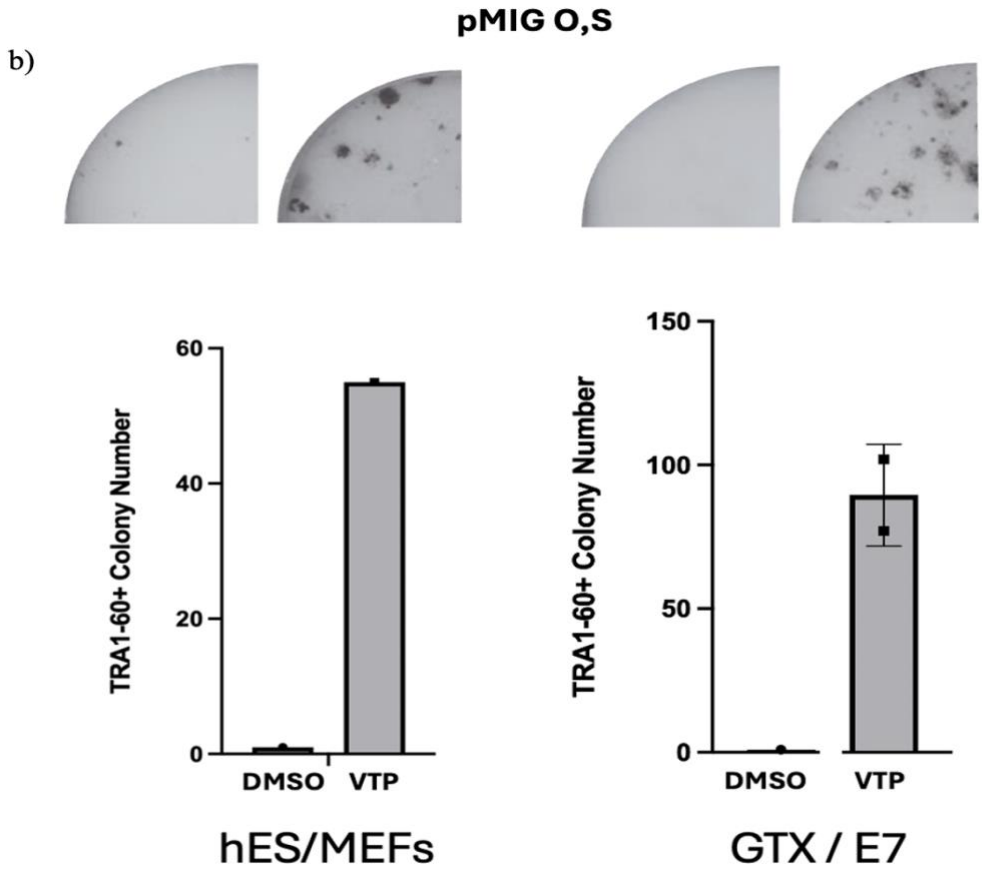

Figure 3.24. TRA 1-60 Positive Colony Numbers following 2-factor (OCT4 and SOX2) Reprogramming. Representative well images and colony numbers are shown for hES/MEF and GTX/E7 primed culture conditions, with both (a) lentiviral and (b) retroviral induction vectors. Error bars represent error of mean. n=2 independent experiments were performed.

3.11 Characterization of MEN1 KO iPSCs

To investigate the impact of MEN1 gene loss on the maintenance of pluripotency, I reprogrammed MEN1 knockout fibroblasts using a lentiviral transgene approach. Then I picked individual colonies and expanded them under mTesr/Geltrex conditions (Figure 3.25). After 5-6 passages, I performed western blot analysis using whole cell lysates derived from five distinct MEN1 knockout clones to confirm the loss of MENIN expression. I observed that none of the five selected clones express MENIN protein indicating that MEN1 loss does not impair either acquisition or the maintenance of human primed pluripotency (Figure 3.26).

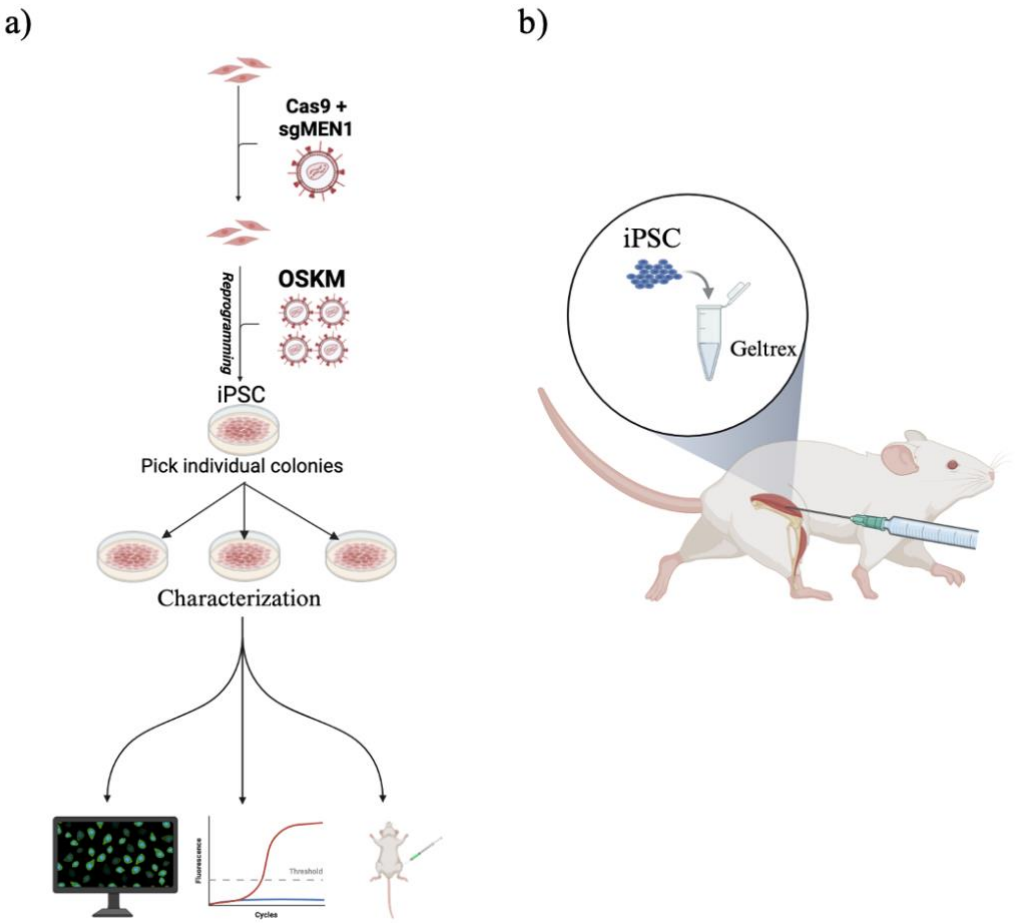

Figure 3.25. (a) Schematic Representation of the Generation and Characterization Process of MEN1 KO iPSC. (b) Schematic Illustration of the intramuscular injection procedure, showing the delivery of iPSC suspended in medium supplemented with Geltrex.

A key hallmark of pluripotency acquisition in iPSCs is the activation and reliance on their endogenous pluripotency network, thus silencing the exogenous factor expression. To test this, I conducted RT-qPCR analysis on selected MEN1 knockout clones. I used primers specifically amplifying the endogenous OCT4, NANOG, KLF4 and C-MYC and the expression levels were normalized to the fibroblasts as a reference. I observed an over 1000-fold increase in expression of OCT4, SOX2, and NANOG, whereas C-MYC expression was completely silenced. KLF4 is highly expressed in fibroblast cells, having comparable levels of expression for our iPSC clones indicates that our clones maintain high expression levels of KLF4 (Figure 3.24).

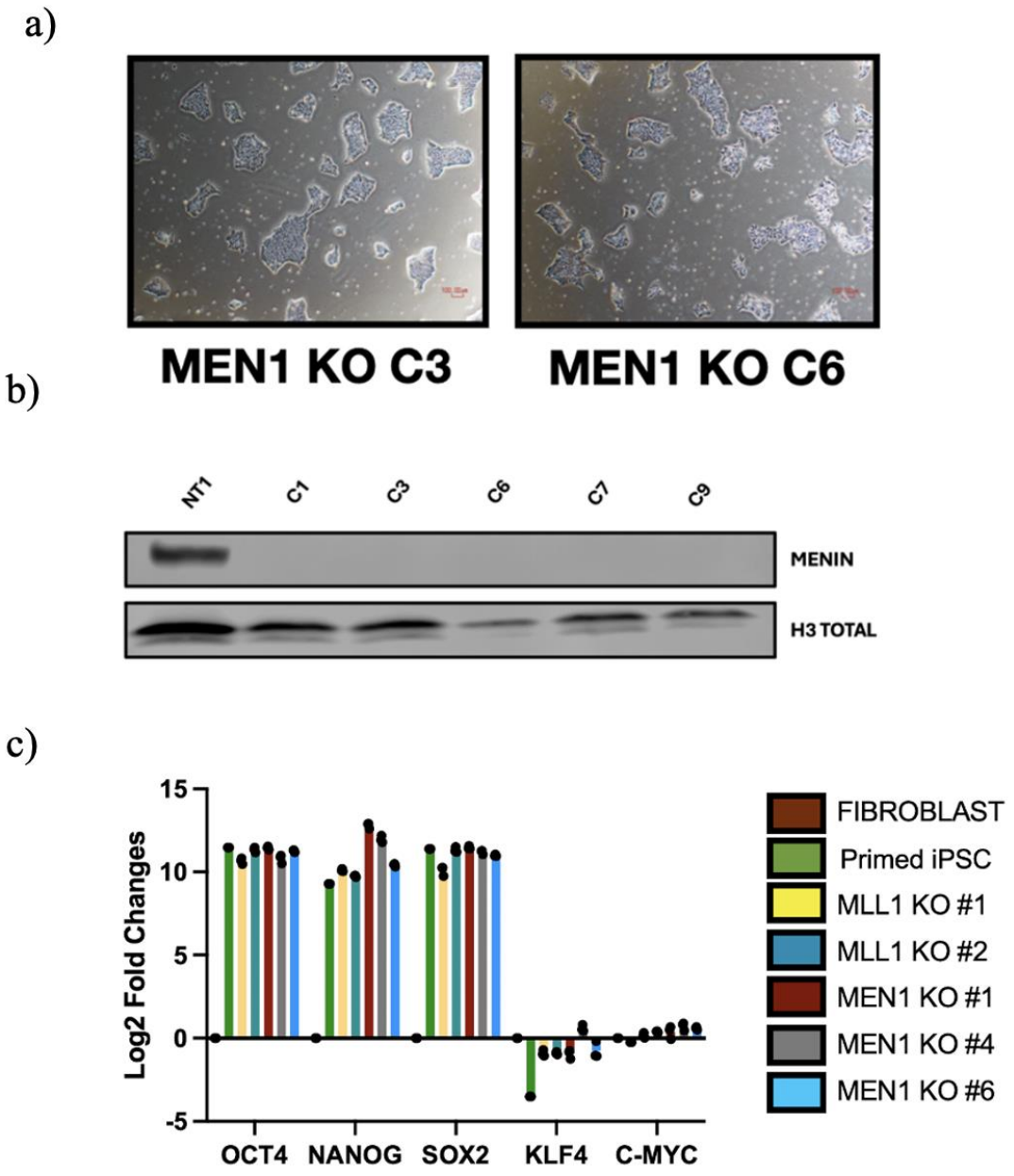

Figure 3.26. (a) Representative phase-contrast images of MEN1 knockout cells cultured under feeder-free primed pluripotency conditions. (b) Western blot results show the MENIN protein levels in each clone. (c) RT-qPCR results show the expression levels of endogenous OCT4, NANOG, SOX2, KLF4 and exogenous c-myc across MEN1 KO and MLL1 KO cell lines. Expression levels are normalized to parental dH1f fibroblasts cell line.

To characterize iPSC clones in terms of their pluripotency and undifferentiated state, I analyzed pluripotency marker expression using immunofluorescence with antibodies against TRA 1-81, OCT4, and SSEA4. I observed high expression levels of all three pluripotency marker proteins, indicating that iPSCs have the characteristic marker expression profile in terms of pluripotent state (Figure 3.27).

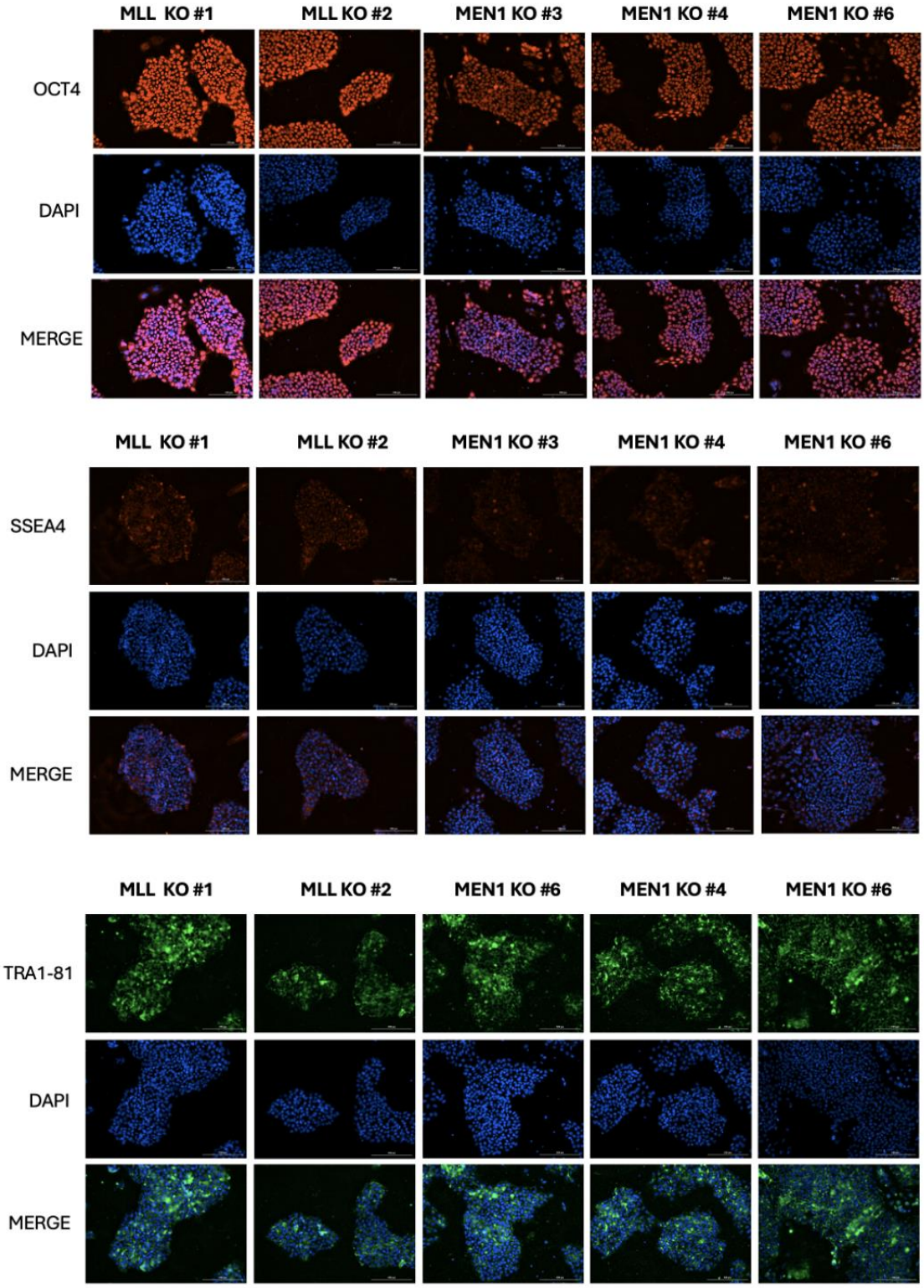

Figure 3.27. Representative immunofluorescence (IF) Images displaying OCT4 (top), SSEA4 (middle) and TRA1-81 (bottom) protein levels of each clone.

Pluripotent stem cells have the capacity to differentiate into all three germ layers. To functionally characterize the iPSCs I performed a teratoma formation assay, in which iPSCs resuspended in serum-containing media supplemented with Geltrex were injected into immunodeficient SCID Mice. Injection was performed intramuscularly to the tibialis posterior muscle. Approximately 2 months after injection, mice were sacrificed and teratomas were collected for further analysis. H&E staining was performed to identify the structures associated with three germ layers. For each clone, glandular areas displaying the endoderm layer, mesenchymal areas showing the presence of mesoderm layer and glial glioneuronal areas revealing the ectodermal layer as labeled respectively (Figure 3.28).

a)

MEN1 C6

MEN1 C4

b)

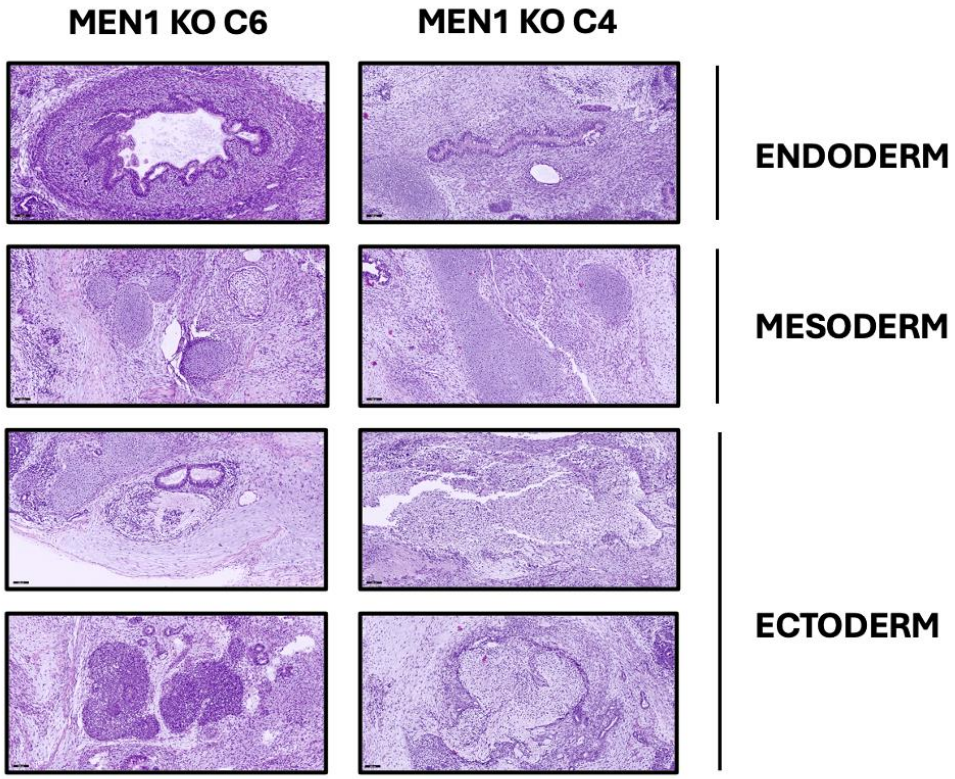

Figure 3.28. (a) Images showing measured diameters and masses of teratomas derived from MEN1 KO iPSC. (b) H&E Staining showing sections of teratomas demonstrating all three germ layers.

CHAPTER 4:
DISCUSSION

Somatic cell reprogramming is inherently a low efficiency process pointing to cell intrinsic barriers to be discovered. Our group performed a perturbation-based CRISPR-Cas9 screen to investigate such barriers (Aztekin,2016). In the first part of this thesis, I focused on USP22, a novel hit from the screen that had been previously validated (Gürhan, 2023). We observed that the loss of USP22, increased reprogramming efficiency by approximately 3-fold. Using a rescue experiment approach, where I reintroduced and overexpressed wild-type USP22 in the USP22 knockout background, I demonstrated that increased reprogramming efficiency was not due to off-target effects but was directly related to the loss of USP22. Given that USP22 is an enzyme that is responsible for catalyzing deubiquitination in the DUB module of SAGA Complex (Bonnet et al., 2008), a point mutant of USP22 lacking catalytic activity was generated (Gürhan, 2023). Upon overexpressing catalytic mutant USP22 in the knockout background, we observed full rescue of the phenotype suggesting that USP22's barrier function is not linked to its catalytic activity. Additionally, catalytic activity of USP22 requires assembly into SAGA Complex (Jeusset & McManus, 2017), so previously in the project, point mutants of USP22, deficient in SAGA complex assembly were generated and reprogrammed (Gürhan, 2023), which resulted in a full rescue of the phenotype, similar to the catalytic mutant. In addition, western blot analysis showed that H2B and H2A mono-ubiquitination levels were comparable in USP22 KO cell lines and all other point mutants, suggesting alternative mechanisms involved in deubiquitination of histones. Alternative to USP22, USP27X and USP51 are two deubiqutinases that are able to form DUBs with ENY2 and ATXN7L3 to deubiquitinate H2B and H2A (Wang et al., 2021). Previously, loss of ENY2 or ATXN7L3 was shown to increase global histone mono-ubiquitination levels making them irreplicable for DUB activity (Gürhan, 2023). Given the potential of redundancy in DUB module formation in USP22 KO Cells, future experiments could investigate whether the increased reprogramming efficiency observed upon USP22 loss related to DUB assembly. Specifically, comparing the reprogramming efficiency of cell lines with knockout adaptor proteins in both USP22 and NT1 backgrounds could reveal whether the phenotype is linked to DUB module assembly.

Beyond its primary role in H2B mono-ubiquitination, our findings indicate that the USP22 loss-mediated enhancement of reprogramming efficiency may be associated to USP22's interaction with proteins that are not SAGA complex member. Since our study primarily focuses on disrupting the catalytic subunits of USP22, it could be worthwhile to explore perturbations in the zinc finger domain, where USP22 interacts with other proteins. Current literature lacks the information on the specific amino acid residues involved in USP22's interactions with non-SAGA member proteins. Functional proteomic approaches such as domain chopping could reveal these residues, deepening our understanding of USP22's interactome and revealing potential new barriers to reprogramming. Finally, developing small molecules targeting these specific interactions could potentially replicate the phenotype of USP22 knockout without requiring transgene expression.

To demonstrate that this phenotype is not restricted to a particular fibroblast cell line and is broadly applicable to all other cell lines, I generated USP22 knockout lines in four primary fibroblast cell lines that were derived from donors by punch biopsy. I observed 2-3-fold increase in reprogramming efficiency under various culture conditions indicating that the phenotype is neither specific to a particular cell line nor dependent on the culture condition used.

Our results showed that USP22 loss leads to upregulation of naïve markers throughout reprogramming. Interestingly, DNMT3L and ALPPL2 exhibit consistent upregulation across all time-points. Furthermore, in primed to naïve conversion experiments, these two markers displayed enhanced upregulation in USP22 KO iPSCs during the early naïve induction phase under both feeder-free and MEF feeder conditions suggesting a closer relationship of USP22 and these genes. To further confirm the relationship between USP22 and these two naïve markers, differentiation assays could be performed using USP22 KO naïve cells to determine whether the loss of USP22 prevents the proper silencing of these naïve pluripotency markers.

Our results also demonstrated that USP22 loss increased the number of naïve colonies generated during naïve reprogramming, consistent with the observed induction of naïve markers during primed reprogramming. Interestingly, we observed heterogeneous naïve cultures at the end of naïve reprogramming. Although some colonies exhibited primed-like morphology, most of them were KLF17 positive. After culturing these cells in naïve conditions for two passages, their morphology transitioned to the expected dome-shaped structure. The persistence of KLF17 expression, even in

differentiated morphology, suggests robust activation of the internal naïve gene network in USP22 KO cells.

To investigate MENIN's negative effect on reprogramming in a time dependent manner, I utilized a doxycycline (dox)-inducible system in which the PAM Mutant MENIN cDNA was cloned into the Fuw-Tet-on vector and transduced into MEN1 KO fibroblast. Using western blot analysis, I demonstrated successful induction of MENIN protein expression upon dox introduction. However, in cells cultured under tet-free serum conditions, I observed slight MENIN expression, indicating leaky activity of the Tet-on system. Surprisingly, as we reprogrammed the generated cell lines, we observed that no-dox condition also rescued the MEN1 KO phenotype suggesting that even the leaky expression of MENIN was sufficient for rescue. Consequently, the transgene-based approach to study MENIN's time dependent negative effect proved unsuitable in our hands. Previously in the project, VTP50469 was utilized to study MENIN's effects in time-dependent manner. However, because VTP50469 specifically targets the MENIN-MLL complex rather than functioning as a MENIN degrader, it failed to provide precise insights into MENIN's MLL-independent effects. Therefore, for future experiments, using specific MENIN degraders in a time-dependent manner could help uncover MENIN's negative effects at distinct timepoints.

Recently discovered MENIN's ability to recognize H3K79me2 mark through its H433 residue (Lin et al., 2023) motivated me to use the point mutant MENIN (H433A), which is deficient in recognizing this chromatin mark. In rescue experiments, I observed a partial rescue of reprogramming phenotype in MEN1 KO cells upon re-introduction of the H433A mutant MENIN, suggesting that MENIN's barrier function is linked to its ability to recognize H3K79me2 modification. Previously, MEN1 KO fibroblasts were reprogrammed under conditions supplemented with inhibitors of DOT1L, a histone methyltransferase that targets H3K79, and is known to repress reprogramming efficiency (Onder et al., 2012). The combined loss of MENIN and DOT1L inhibition did not produce an additive effect on reprogramming efficiency (Yilmaz, 2023) suggesting a relationship between MEN1-loss mediated enhanced reprogramming and H3K79me2/me3 chromatin mark deposition. Reprogramming the H433A Mutant with a DOT1L inhibitor could further support the hypothesis of MENIN's partial dependence on H3K79me2 recognition if H433A, when combined with DOT1L inhibitor still partially rescues the MEN1 KO phenotype.

In our group's CRISPR-Cas9-based screen, which identified USP22 as a novel barrier, genetically modified fibroblasts were reprogrammed in the presence of DOT1L inhibitor to enhance reprogramming efficiency (Aztekin,2016). Subsequent validation experiments revealed that DOT1L inhibition further enhances reprogramming efficiency of USP22 KO fibroblasts, suggesting that the two chromatin modifiers operate through independent mechanisms (Gürhan, 2023). Since DOT1L inhibition does not further enhance reprogramming efficiency of MEN1 KO fibroblasts, suggesting a shared mechanism of action (Yilmaz, 2023), we speculate that simultaneous perturbation of USP22 and MENIN may result in additive enhancement of reprogramming efficiency. Therefore, future experiments involving the simultaneous perturbation of MENIN and USP22 could determine whether these two chromatin factors act as independent barriers. It is crucial to identify such barriers which function in distinct epigenetic context and developing small molecule inhibitors to target them or their interactions, since one of the aims of the reprogramming field is to replace OSKM factors with chemical alternatives.

Since the Yamanaka et.al introduced the first transcription-factor mediated reprogramming, the overarching goal of the field has been to replace all transcription factors with small molecules to obtain transgene-free iPSCs. To date, two studies have reported successful chemical reprogramming in human cells (Guan et al., 2022, Liuyang et al., 2023). VTP50469 is one of the chemicals in the chemical reprogramming cocktail, pointing to the importance of the MENIN-MLL complex in reprogramming process. I demonstrated that VTP50469 can replace the KLF4 and C-MYC transcription factors; however, in my experiments, reprogramming with overexpression of only one factor (either OCT4 or SOX2) with VTP50469 supplementation failed to generate iPSCs, suggesting that VTP50469 alone cannot independently substitute for both pillar factors.

BIBLIOGRAPHY

Agarwal, S. K. (2013). Multiple Endocrine Neoplasia Type 1. Frontiers of Hormone Research, 1–15. https://doi.org/10.1159/000345666

Agarwal, S. K. (2013b). Multiple Endocrine Neoplasia Type 1. Frontiers of Hormone Research, 1–15. https://doi.org/10.1159/000345666

Agarwal, S. K., Guru, S. C., Heppner, C., Erdos, M. R., Collins, R. M., Park, S. Y., Saggar, S., Chandrasekharappa, S. C., Collins, F. S., Spiegel, A. M., Marx, S. J., & Burns, A. (1999). Menin Interacts with the AP1 Transcription Factor JunD and Represses JunD-Activated Transcription. Cell, 96(1), 143–152. https://doi.org/10.1016/s0092-8674(00)80967-8

Apostolou, E., & Hochedlinger, K. (2013). Chromatin dynamics during cellular reprogramming. Nature, 502(7472), 462–471. https://doi.org/10.1038/nature12749

Arabacı, D. H., Terzioğlu, G., Bayırbaşı, B., & Önder, T. T. (2020). Going up the hill: chromatin-based barriers to epigenetic reprogramming. FEBS Journal, 288(16), 4798–4811. https://doi.org/10.1111/febs.15628

Bayerl, J., Ayyash, M., Shani, T., Manor, Y. S., Gafni, O., Massarwa, R., Kalma, Y., Aguilera-Castrejon, A., Zerbib, M., Amir, H., Sheban, D., Geula, S., Mor, N., Weinberger, L., Tassa, S. N., Krupalnik, V., Oldak, B., Livnat, N., Tarazi, S., . . . Hanna, J. H. (2021). Principles of signaling pathway modulation for enhancing human naive pluripotency induction. *Cell Stem Cell*, *28*(9), 1549-1565.e12. https://doi.org/10.1016/j.stem.2021.04.001

Bonnet, J., Romier, C., Tora, L., & Devys, D. (2008). Zinc-finger UBPs: regulators of deubiquitylation. Trends in Biochemical Sciences, 33(8), 369–375. https://doi.org/10.1016/j.tibs.2008.05.005

Cerneckis, J., Cai, H., & Shi, Y. (2024). Induced pluripotent stem cells (iPSCs): molecular mechanisms of induction and applications. *Signal Transduction and Targeted Therapy*, *9*(1). https://doi.org/10.1038/s41392-024-01809-0

Collier, A. J., & Rugg-Gunn, P. J. (2018). Identifying Human Naïve Pluripotent Stem Cells − Evaluating State-Specific Reporter Lines and Cell-Surface Markers. BioEssays, 40(5). https://doi.org/10.1002/bies.201700239

Dalton, S. (2012). Signaling networks in human pluripotent stem cells. *Current Opinion in Cell Biology*, *25*(2), 241–246. https://doi.org/10.1016/j.ceb.2012.09.005

Daniel, J. A., & Grant, P. A. (2007). Multi-tasking on chromatin with the SAGA coactivator complexes. Mutation Research/Fundamental and Molecular Mechanisms of Mutagenesis, 618(1–2), 135–148. https://doi.org/10.1016/j.mrfmmm.2006.09.008

De Carvalho, D. D., You, J. S., & Jones, P. A. (2010). DNA methylation and cellular reprogramming. Trends in Cell Biology, 20(10), 609–617. https://doi.org/10.1016/j.tcb.2010.08.003

Dong, C., Fischer, L. A., & Theunissen, T. W. (2019). Recent insights into the naïve state of human pluripotency and its applications. *Experimental Cell Research*, *385*(1), 111645. https://doi.org/10.1016/j.yexcr.2019.111645

Du, P., & Wu, J. (2024). Hallmarks of totipotent and pluripotent stem cell states. *Cell Stem Cell*, *31*(3), 312–333. https://doi.org/10.1016/j.stem.2024.01.009

Ebrahimi, A., Sevinç, K., Sevinç, G. G., Cribbs, A. P., Philpott, M., Uyulur, F., Morova, T., Dunford, J. E., Göklemez, S., Arı, Ş., Oppermann, U., & Önder, T. T. (2019). Bromodomain inhibition of the coactivators CBP/EP300 facilitate cellular reprogramming. Nature Chemical Biology, 15(5), 519–528. https://doi.org/10.1038/s41589-019-0264-z

Ehrensberger, A. H., & Svejstrup, J. Q. (2012). Reprogramming chromatin. Critical Reviews in Biochemistry and Molecular Biology, 47(5), 464–482. https://doi.org/10.3109/10409238.2012.697125

Glickman, M. H., & Ciechanover, A. (2002). The Ubiquitin-Proteasome Proteolytic Pathway: Destruction for the Sake of Construction. Physiological Reviews, 82(2), 373–428. https://doi.org/10.1152/physrev.00027.2001

Gobl, A. E., Berg, M., Lopez-Egido, J. R., Öberg, K., Skogseid, B., & Westin, G. (1999). Menin represses JunD-activated transcription by a histone deacetylase-dependent mechanism. Biochimica Et Biophysica Acta (BBA) - Gene Structure and Expression, 1447(1), 51–56. https://doi.org/10.1016/s0167-4781(99)00132-3

Guan, J., Wang, G., Wang, J., Zhang, Z., Fu, Y., Cheng, L., Meng, G., Lyu, Y., Zhu, J., Hanna, J., Cheng, A. W., Saha, K., Kim, J., Lengner, C. J., Soldner, F., Cassady, J. P., Muffat, J., Carey, B. W., & Jaenisch, R. (2010). Human embryonic stem cells with biological and epigenetic characteristics similar to those of mouse ESCs. *Proceedings of the National Academy of Sciences*, *107*(20), 9222–9227. https://doi.org/10.1073/pnas.1004584107

Huang, J., Gurung, B., Wan, B., Matkar, S., Veniaminova, N. A., Wan, K., Merchant, J. L., Hua, X., & Lei, M. (2012). The same pocket in menin binds both MLL and JUND

but has opposite effects on transcription. Nature, 482(7386), 542–546. https://doi.org/10.1038/nature10806

Jeusset, L., & McManus, K. (2017). Ubiquitin specific peptidase 22 regulates Histone H2B Mono-Ubiquitination and exhibits both oncogenic and tumor suppressor roles in cancer. Cancers, 9(12), 167. https://doi.org/10.3390/cancers9120167

Krivtsov, A. V., Evans, K., Gadrey, J. Y., Eschle, B. K., Hatton, C., Uckelmann, H. J., Ross, K. N., Perner, F., Olsen, S. N., Pritchard, T., McDermott, L., Jones, C. D., Jing, D., Braytee, A., Chacon, D., Earley, E., McKeever, B. M., Claremon, D., Gifford, A. J., . . . Armstrong, S. A. (2019). A Menin-MLL Inhibitor Induces Specific Chromatin Changes and Eradicates Disease in Models of MLL-Rearranged Leukemia. Cancer Cell, 36(6), 660-673.e11. https://doi.org/10.1016/j.ccell.2019.11.001

Lea, R. A., McCarthy, A., Boeing, S., Fallesen, T., Elder, K., Snell, P., Christie, L., Adkins, S., Shaikly, V., Taranissi, M., & Niakan, K. K. (2021). KLF17 promotes human naïve pluripotency but is not required for its establishment. Development, 148(22). https://doi.org/10.1242/dev.199378

Lehmann, R., Lee, C. M., Shugart, E. C., Benedetti, M., Charo, R. A., Gartner, Z., Hogan, B., Knoblich, J., Nelson, C. M., & Wilson, K. M. (2019). Human organoids: a new dimension in cell biology. Molecular Biology of the Cell, 30(10), 1129–1137. https://doi.org/10.1091/mbc.e19-03-0135

Li, Y., Wang, Y., Liuyang, S., Liu, B., Yang, Z., He, H., Zhong, X., Chen, Q., Zhang, X., Sun, S., . . . Deng, H. (2022). Chemical reprogramming of human somatic cells to pluripotent stem cells. Nature, 605(7909), 325–331. https://doi.org/10.1038/s41586-022-04593-5

Lin, J., Wu, Y., Tian, G., Yu, D., Yang, E., Lam, W. H., Liu, Z., Jing, Y., Dang, S., Bao, X., Wong, J. W. H., Zhai, Y., & Li, X. D. (2023). Menin “reads” H3K79me2 mark in a nucleosomal context. Science, 379(6633), 717–723. https://doi.org/10.1126/science.adc9318

Liuyang, S., Wang, G., Wang, Y., He, H., Lyu, Y., Cheng, L., Yang, Z., Guan, J., Fu, Y., Zhu, J., Zhong, X., Sun, S., Li, C., Wang, J., & Deng, H. (2023). Highly efficient and rapid generation of human pluripotent stem cells by chemical reprogramming. Cell Stem Cell, 30(4), 450-459.e9. https://doi.org/10.1016/j.stem.2023.02.008

Matkar, S., Thiel, A., & Hua, X. (2013). Menin: a scaffold protein that controls gene expression and cell signaling. Trends in Biochemical Sciences, 38(8), 394–402. https://doi.org/10.1016/j.tibs.2013.05.005

Melo-Cardenas, J., Zhang, Y., Zhang, D. D., & Fang, D. (2016). Ubiquitin-specific peptidase 22 functions and its involvement in disease. Oncotarget, 7(28), 44848–44856. https://doi.org/10.18632/oncotarget.8602

Michlits, G., Hubmann, M., Wu, S., Vainorius, G., Budusan, E., Zhuk, S., Burkard, T. R., Novatchkova, M., Aichinger, M., Lu, Y., Reece-Hoyes, J., Nitsch, R., Schramek, D., Hoepfner, D., & Elling, U. (2017). CRISPR-UMI: single-cell lineage tracing of pooled CRISPR–Cas9 screens. Nature Methods, 14(12), 1191–1197. https://doi.org/10.1038/nmeth.4466

Miles, D. C., De Vries, N. A., Gisler, S., Lieftink, C., Akhtar, W., Gogola, E., Pawlitzky, I., Hulsman, D., Tanger, E., Koppens, M., Beijersbergen, R. L., & Van Lohuizen, M. (2016). TRIM28 Is an Epigenetic Barrier to Induced Pluripotent Stem Cell Reprogramming. Stem Cells, 35(1), 147–157. https://doi.org/10.1002/stem.2453

Miyabayashi, T., Teo, J., Yamamoto, M., McMillan, M., Nguyen, C., & Kahn, M. (2007). Wnt/β-catenin/CBP signaling maintains long-term murine embryonic stem cell pluripotency. Proceedings of the National Academy of Sciences, 104(13), 5668–5673. https://doi.org/10.1073/pnas.0701331104

Murai, M. J., Chruszcz, M., Reddy, G., Grembecka, J., & Cierpicki, T. (2011). Crystal Structure of Menin Reveals Binding Site for Mixed Lineage Leukemia (MLL) Protein. Journal of Biological Chemistry, 286(36), 31742–31748. https://doi.org/10.1074/jbc.m111.258186

Onder, T. T., Kara, N., Cherry, A., Sinha, A. U., Zhu, N., Bernt, K. M., Cahan, P., Mancarci, B. O., Unternaehrer, J., Gupta, P. B., Lander, E. S., Armstrong, S. A., & Daley, G. Q. (2012). Chromatin-modifying enzymes as modulators of reprogramming. Nature, 483(7391), 598–602. https://doi.org/10.1038/nature10953

Piret, S. E., & Thakker, R. V. (2011). Mouse models for inherited endocrine and metabolic disorders. Journal of Endocrinology, 211(3), 211–230. https://doi.org/10.1530/joe-11-0193

Piret, S. E., & Thakker, R. V. (2011b). Mouse models for inherited endocrine and metabolic disorders. Journal of Endocrinology, 211(3), 211–230. https://doi.org/10.1530/joe-11-0193

Popowski, M. (2015). Repressors of reprogramming. World Journal of Stem Cells, 7(3), 541. https://doi.org/10.4252/wjsc.v7.i3.541

Qin, H., Diaz, A., Blouin, L., Lebbink, R. J., Patena, W., Tanbun, P., LeProust, E. M., McManus, M. T., Song, J. S., & Ramalho-Santos, M. (2014). Systematic Identification

of Barriers to Human iPSC Generation. Cell, 158(2), 449–461. https://doi.org/10.1016/j.cell.2014.05.040

Reyes-Turcu, F. E., Ventii, K. H., & Wilkinson, K. D. (2009). Regulation and Cellular Roles of Ubiquitin-Specific Deubiquitinating Enzymes. Annual Review of Biochemistry, 78(1), 363–397. https://doi.org/10.1146/annurev.biochem.78.082307.091526

Rulifson, I. C., Karnik, S. K., Heiser, P. W., Berge, D. T., Chen, H., Gu, X., Taketo, M. M., Nusse, R., Hebrok, M., & Kim, S. K. (2007). Wnt signaling regulates pancreatic β cell proliferation. Proceedings of the National Academy of Sciences, 104(15), 6247–6252. https://doi.org/10.1073/pnas.0701509104

Sowa, M. E., Bennett, E. J., Gygi, S. P., & Harper, J. W. (2009). Defining the Human Deubiquitinating Enzyme Interaction Landscape. Cell, 138(2), 389–403. https://doi.org/10.1016/j.cell.2009.04.042

Stuart, H. T., Van Oosten, A. L., Radzisheuskaya, A., Martello, G., Miller, A., Dietmann, S., Nichols, J., & Silva, J. C. (2014). NANOG amplifies STAT3 activation and they synergistically induce the naive pluripotent program. Current Biology, 24(3), 340–346. https://doi.org/10.1016/j.cub.2013.12.040

Takahashi, K., & Yamanaka, S. (2015). A developmental framework for induced pluripotency. Development, 142(19), 3274–3285. https://doi.org/10.1242/dev.114249

Takahashi, S., Kobayashi, S., & Hiratani, I. (2017). Epigenetic differences between naïve and primed pluripotent stem cells. *Cellular and Molecular Life Sciences*, *75*(7), 1191–1203. https://doi.org/10.1007/s00018-017-2703-x

Takashima, Y., Guo, G., Loos, R., Nichols, J., Ficz, G., Krueger, F., Oxley, D., Santos, F., Clarke, J., Mansfield, W., Reik, W., Bertone, P., & Smith, A. (2014). Resetting Transcription Factor Control Circuitry toward Ground-State Pluripotency in Human. *Cell*, *158*(6), 1254–1269. https://doi.org/10.1016/j.cell.2014.08.029

Wang, F., El-Saafin, F., Ye, T., Stierle, M., Negroni, L., Durik, M., Fischer, V., Devys, D., Vincent, S. D., & Tora, L. (2021). Histone H2Bub1 deubiquitylation is essential for mouse development, but does not regulate global RNA polymerase II transcription. Cell Death and Differentiation, 28(8), 2385–2403. https://doi.org/10.1038/s41418-021-00759-2

Weinberger, L., Ayyash, M., Novershtern, N., & Hanna, J. H. (2016). Dynamic stem cell states: naive to primed pluripotency in rodents and humans. *Nature Reviews Molecular Cell Biology*, *17*(3), 155–169. https://doi.org/10.1038/nrm.2015.28

Wiegand, C., & Banerjee, I. (2019). Recent advances in the applications of iPSC technology. *Current Opinion in Biotechnology*, *60*, 250–258. https://doi.org/10.1016/j.copbio.2019.05.011

Yamane, M., Ohtsuka, S., Matsuura, K., Nakamura, A., & Niwa, H. (2018c). Overlapping functions of Krüppel-like factor family members: targeting multiple transcription factors to maintain the naïve pluripotency of mouse embryonic stem cells. Development, 145(10). https://doi.org/10.1242/dev.162404

Yang, C., Chang, K., & Rana, T. M. (2014). Genome-wide Functional Analysis Reveals Factors Needed at the Transition Steps of Induced Reprogramming. Cell Reports, 8(2), 327–337. https://doi.org/10.1016/j.celrep.2014.07.002

Yokoyama, A., & Cleary, M. L. (2008). Menin Critically Links MLL Proteins with LEDGF on Cancer-Associated Target Genes. Cancer Cell, 14(1), 36–46. https://doi.org/10.1016/j.ccr.2008.05.003

Yokoyama, A., Wang, Z., Wysocka, J., Sanyal, M., Aufiero, D. J., Kitabayashi, I., Herr, W., & Cleary, M. L. (2004). Leukemia Proto-Oncoprotein MLL Forms a SET1-Like Histone Methyltransferase Complex with Menin To Regulate Hox Gene Expression. Molecular and Cellular Biology, 24(13), 5639–5649. https://doi.org/10.1128/mcb.24.13.5639-5649.2004

APPENDIX A

MENIN is a nuclear scaffold protein that interacts with a variety of other proteins, predominantly transcription factors and chromatin modifiers. In order to determine the interaction between such proteins contributing to the MENIN being a barrier to reprogramming, we selected two well characterized interaction partners including transcription factor JUND and the histone methyltransferase KMT2B. We designed and cloned three different sgRNAs targeting each gene into plenticriscrpV2 followed by lentiviral transduction to NT1 and MEN1 KO fibroblasts. We confirmed the reduction in mRNA expression levels for each gene with qPCR (Figure A.1). Subsequently, generated cell lines are reprogrammed using OSKM induction, but unfortunately cells expressing NT1 Cas9 failed to survive OSKM induction whereas MEN1 KO Cells successfully generated iPSC colonies.

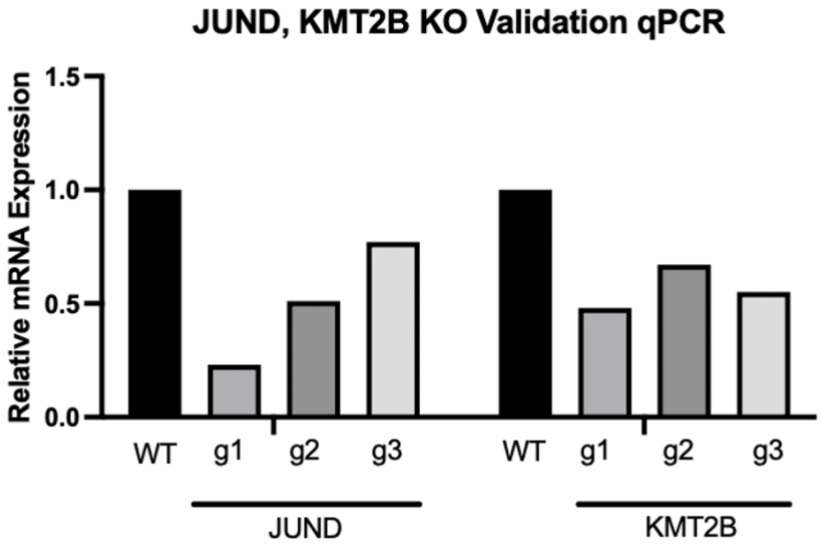

Figure A.1. Relative mRNA expression levels of NT1 fibroblast cell lines transduced with three independent sgRNAs targeting JUND and KMT2B.

According to our hypothesis, increased reprogramming efficiency upon double knock-out would suggest that the barrier function of these proteins is independent of MENIN interaction. Conversely, absence of such increase would indicate that proteins impede reprogramming via interacting with MENIN. We observed a slight increase for

both double knock-out groups (Figure A.2 and Figure A.3) but because of the loss of NT1 cells, our results remained inconclusive.

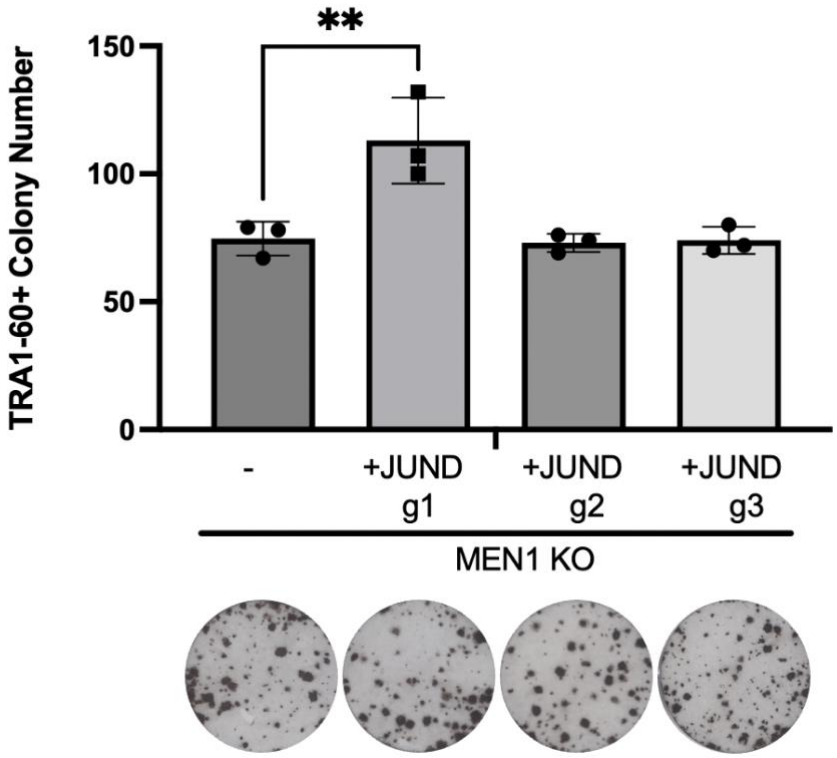

Figure A.2. TRA-1-60 Positive Colony Numbers at the end of reprogramming after transducing cells with three independent sgRNA targeting JUND on MEN1 KO background. Error bars indicate the error of mean. n=3, independent experiments were performed. * Stands for $p \leq 0.05$

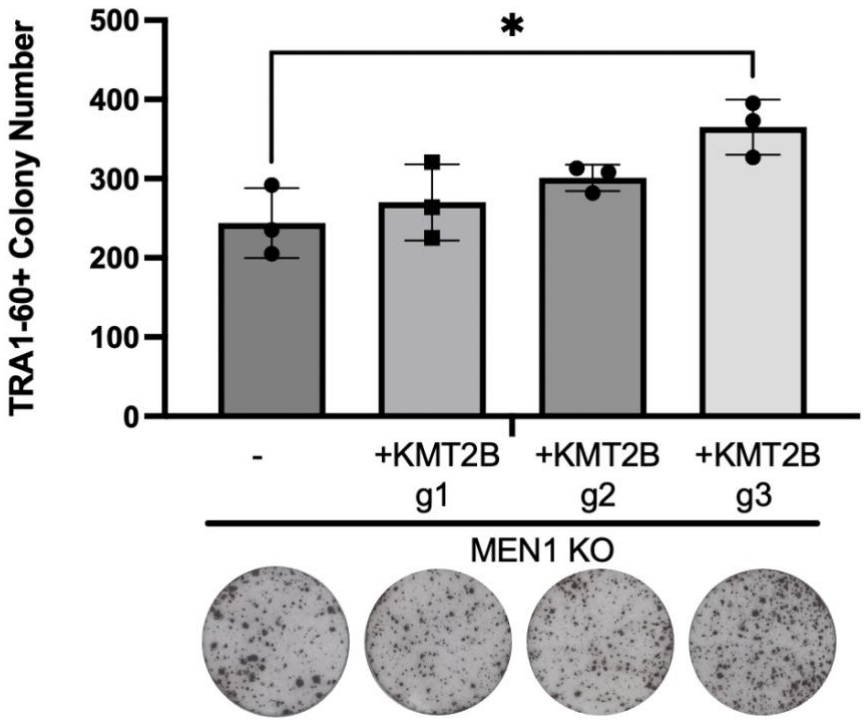

Figure A.3. TRA-1-60 Positive Colony Numbers at the end of reprogramming after transducing cells with three independent sgRNA targeting KMT2B on MEN1 KO background. Error bars indicate the error of mean. n=3, independent experiments were performed. * Stands for $p \leq 0.05$.

Moreover, we evaluated two novel MENIN degrader chemicals called MT1, MT2. First, we treated fibroblast cells with each chemical for 24,48 and 72 hours with varying concentrations and checked the MENIN protein expression using Western Blot Analysis. We did not observe any significant signal reduction for MT1 for both 24- and 48-hours treatment, whereas we observed modest signal reduction in MT2 treated cells.

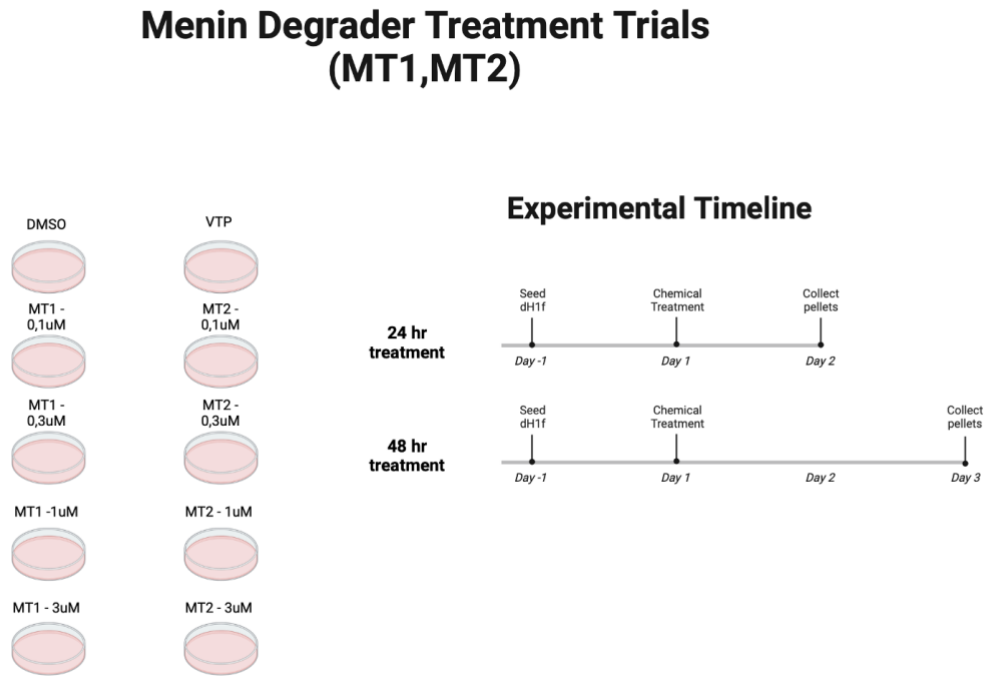

Figure **A.4.** Schematics of MT-1 and MT-2 Chemical Treatment Strategy.

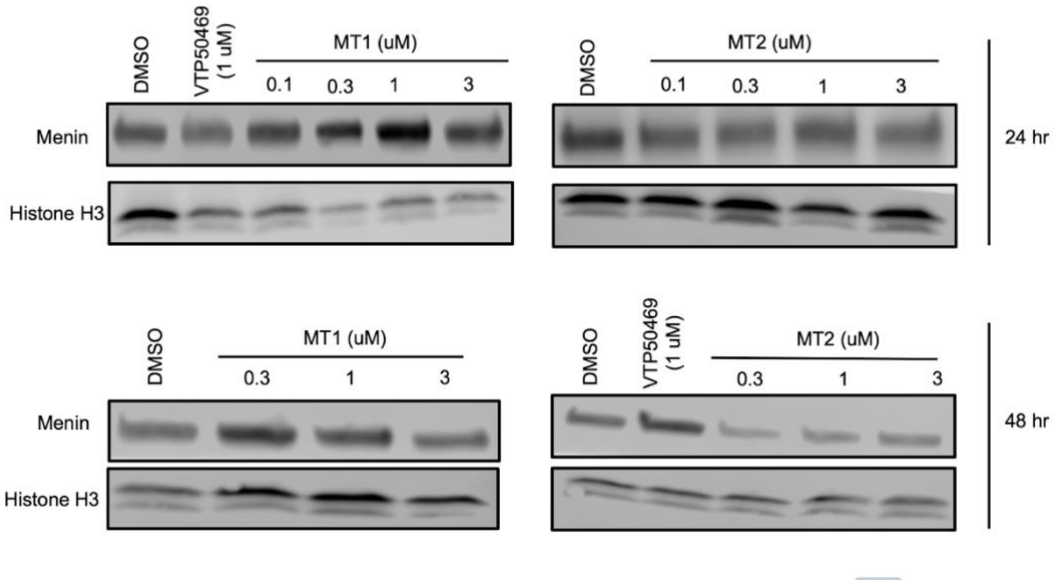

Figure A.5. Western Blot Images showing MENIN Expression Levels after MT1, MT2 treatment with varying concentrations for 24 and 48 hours.

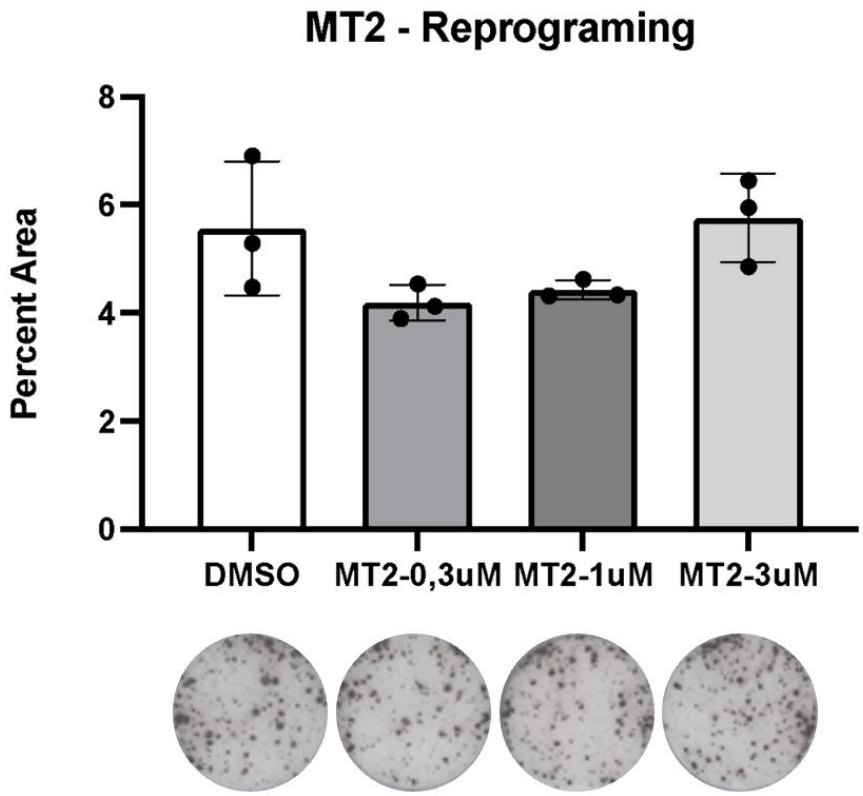

Figure A.6. Percent Area covered by TRA-1-60 positive colonies at the end of Reprogramming. Error bars indicate the error of mean. n=3, independent experiments were performed.

So, we reprogrammed the fibroblast cells using various concentrations of MT2, replenishing it every 48 hours. Unfortunately, we did not observe any significant change in reprogramming efficiency as indicated by quantified TRA 1-60 positive colony number. (Figure A.6) Since we know that MEN1 KO greatly increases the reprogramming efficiency, we suggest that MT-2 does not induce sufficient decrease in MENIN expression levels to impact reprogramming.